Tricritical behavior in the extended Hubbard chains

Masaaki Nakamura*

Institute for Solid State Physics, University of Tokyo, Roppongi, Tokyo 106-8666, Japan
(Received 15 September 1999; revised manuscript received 2 February 2000)

Phase diagrams of the one-dimensional extended Hubbard model (including nearest-neighbor interaction V) at half- and quarter-filling are studied by observing level crossings of excitation spectra using the exact diagonalization. This method is based on the Tomonaga-Luttinger liquid theory including logarithmic corrections which stem from the renormalization of the Umklapp- and the backward-scattering effects. Using this approach, the phase boundaries are determined with high accuracy, and then the structure of the phase diagram is clarified. At half-filling, the phase diagram consists of two Berezinskii-Kosterlitz-Thouless (BKT) transition lines and one Gaussian transition line in the charge sector, and one spin-gap transition line. This structure reflects the $U(1) \otimes SU(2)$ symmetry of the electron system. Near the $U = 2V$ line, the Gaussian and the spin-gap transitions take place independently from the weak- to the intermediate-coupling region, but these two transition lines are coupled in the strong-coupling region. This result demonstrates existence of a tricritical point and a bond-charge-density-wave (BCDW) phase between charge- and spin-density-wave (CDW, SDW) phases. To clarify this mechanism of the transition, we also investigate effect of a correlated hopping term, which plays a role to enlarge BCDW and bond-spin-density-wave (BSDW) phases. At quarter-filling, a similar crossover phenomenon also takes place in the large-V region involving spin-gap and BKT-type metal-insulator transitions.

I. INTRODUCTION

One-dimensional (1D) electron systems have been extensively studied motivated not only by theoretical interest but also by the discovery of quasi-1D conductors and high-T_c superconductivity. In the 1D electron systems, due to the charge-spin separation, the low-energy excitations in the charge and the spin sectors may have gaps independently, and then various phases can appear. However, phenomena caused by interplay between these two degrees of freedom have not been fully understood even in simple models. In this paper, we turn our attention to the phase transitions in the so-called extended Hubbard model (EHM),

$$\mathcal{H}_{EHM} = -t \sum_{is} (c_{is}^\dagger c_{i+1,s} + \text{H.c.}) + U \sum_i n_{i\uparrow} n_{i\downarrow}$$

$$+ V \sum_i n_i n_{i+1}, \qquad (1)$$

at half- and quarter-filling, where both charge and spin gaps can open.

The EHM at half-filling has been studied using various approaches. In the weak-coupling limit, the phase diagram is analytically obtained by the g-ology[1–4] (see Appendix A). According to the result, there appear insulating charge- (CDW) and spin-density-wave (SDW) phases, or metallic phases where the singlet superconducting (SS) and the triplet superconducting (TS) correlation is dominant [see Fig. 1(b)]. On the other hand, in the strong-coupling limit, the perturbation theory gives the phase boundary of the CDW-SDW transition[5–7] and of the phase separation.[8–10] The rest of region has been discussed by numerical analysis.[6,11–15] However, the phase diagrams are not fully understood, because the charge and the spin gaps open exponentially slow [see

Eqs. (18) and (21)], which makes it difficult to determine the phase boundaries by the conventional finite-size scaling method. Especially for the transition between the CDW and the SDW phases, even the property of the transition itself is not clear, because the transition is of the second order in the weak-coupling theory, while it is of the first order in the strong-coupling theory.

Recently, the author has clarified the mechanism of the CDW-SDW transition.[16] According to the result, the phase boundary consists of two independent transition lines, and the crossover of the CDW-SDW transition is related with whether these two transition lines are separated or coupled. The result also demonstrates the existence of the bond-charge-density-wave (BCDW)[17] phase in the very narrow region between the CDW and the SDW states. In this paper, we not only give the details of the letter, but also clarify the entire phase diagram of the EHM at half-filling.

In order to clarify the above scenario for the phase transition between the CDW and the SDW phases, we also con-
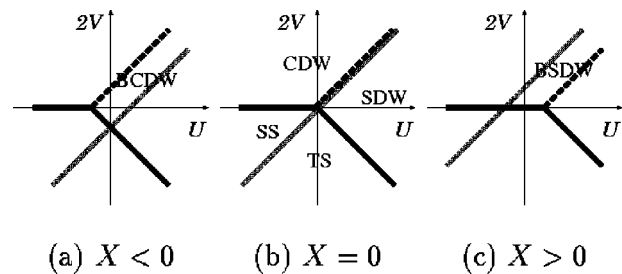

FIG. 1. Weak-coupling phase diagrams of the EHM including the correlated hopping term (Ref. 20). The phase diagrams are given by combinations of a Y-shaped structure for the charge part [two BKT lines (solid) and one Gaussian line (dashed)] and an I-shaped one for the spin part.

sider generalizing the EHM by adding the following correlated hopping interactions:[18–20,21]

$$\mathcal{H}_X = X \sum_{is} (c_{is}^\dagger c_{i+1,s} + \text{H.c.})(n_{i,-s} - n_{i+1,-s})^2. \quad (2)$$

This interaction can be derived as a site-off-diagonal element of the Coulomb integral.[18] Especially, the three-body part is justified as an effective interaction in the three-band model.[19] The weak-coupling phase diagram is known by the g-ology[20] as shown in Figs. 1(a) and 1(c) (see Appendix A). In these phase diagrams, the two transition lines between the CDW and the SDW phases do not synchronize. And a BCDW or a bond-spin-density-wave[22] (BSDW) phase appears. The analysis of the generalized model will clarify the tricritical behavior in the pure EHM. The final results are shown in Fig. 15.

A charge-gap phase is known to appear not only at half-filling but also at quarter-filling,[23–26] due to the effect of the Umklapp scattering in the higher order.[27–30] In this case, the interplay between charge and spin instabilities is also expected. In fact, we will conclude that a crossover phenomenon also exists in the large-V region at quarter-filling (see Fig. 16).

Throughout this paper, we use the level-crossing approach to determine the phase boundaries.[16,31–37] This method is based on the Tomonaga-Luttinger (TL) liquid theory[38] (which is equivalent to the $c=1$ conformal field theory) including the logarithmic corrections, which stem from the renormalization of the Umklapp- and the backward-scattering effects. In the theoretical scheme, the transition points are identified by the level crossing of the excitation spectra in the finite-size ring with size dependence $\mathcal{O}(L^{-2})$, where L is the system size. Therefore, the phase boundaries are obtained with high accuracy, using the numerical data of finite-size clusters.

This paper is organized as follows. In Sec. II, we review the level-crossing approach based on the TL liquid theory and the renormalization group, developed in Refs. 31–36. In Sec. III, we discuss the discrete symmetries of wave functions to connect excitation spectra and the corresponding physical states. In Sec. IV, we discuss the character of the phases that appear in the phase diagrams. In Sec. V, we analyze the instabilities of the EHM at half-filling, and clarify the phase diagram. In Sec. VI, we analyze the metal-insulator transition at quarter-filling. Finally, a summary and discussions are given in Sec. VII. In Appendix A, we briefly explain the traditional g-ology analysis for the generalized EHM at half-filling.

II. PHASE BOUNDARIES

First, let us perform a general argument for 1D electron systems based on the bosonization theory.[1–4,39,40] The continuous fermion fields are defined by $c_{js}/\sqrt{a} \to \psi_{L,s}(x) + \psi_{R,s}(x)$ (the lattice constant $a \to 0$, $x = ja$) with

$$\psi_{r,s}(x) = \frac{U_{r,s}}{\sqrt{2\pi\alpha}} e^{irk_F x} e^{i/\sqrt{2}[r(\phi_\rho + s\phi_\sigma) - \theta_\rho - s\theta_\sigma]}, \quad (3)$$

where $r = \text{R, L}$ and $s = \uparrow, \downarrow$ refer to $+$ and $-$ in that order. α is a short-distance cutoff. k_F is the Fermi wave number de-

fined by $k_F \equiv \pi n/2$, with n being the electron density. The field ϕ_ν and the dual field θ_ν of the charge ($\nu = \rho$) and the spin ($\nu = \sigma$) degrees of freedom satisfy the relation

$$[\phi_\mu(x), \theta_\nu(x')] = -\frac{i\pi}{2} \delta_{\mu\nu} \, \text{sgn}(x - x'). \quad (4)$$

$U_{r,s}$ ensures anticommutation relations of the different fermion fields.[38,40] These operators are Hermitian and satisfy the relation

$$\{U_{r,s}, U_{r',s'}\} = 2\delta_{r,r'}\delta_{s,s'}. \quad (5)$$

Using the formalism, the low-energy behavior of 1D electron system can be described by the sine-Gordon models for the charge and the spin sectors. When $2q$ (q: integer) electrons contribute to the Umklapp scattering, the effective Hamiltonian for the system with length L is given by

$$\mathcal{H} = \sum_{\nu=\rho,\sigma} \frac{v_\nu}{2\pi} \int_0^L dx [K_\nu(\partial_x\theta_\nu)^2 + K_\nu^{-1}(\partial_x\phi_\nu)^2]$$

$$+ \frac{2g_{1\perp}}{(2\pi\alpha)^2} \int_0^L dx \cos[\sqrt{8}\phi_\sigma(x)]$$

$$+ \frac{2g_{3\perp}}{(2\pi\alpha)^2} \int_0^L dx \cos[q\sqrt{8}\phi_\rho(x) + \delta x]$$

$$+ \frac{2g_{3\parallel}}{(2\pi\alpha)^2} \int_0^L dx \cos[q\sqrt{8}\phi_\rho(x) + \delta x]\cos[\sqrt{8}\phi_\sigma(x)], \quad (6)$$

where v_ν and K_ν are the velocity and the Gaussian coupling, respectively for each sector. $g_{1\perp}$ and $g_{3\perp}$ denote the amplitude of the backward and the Umklapp scattering, respectively. The Umklapp term vanishes except for the case $\delta \equiv 2p\pi - 4qk_F = 0$, where p is also an integer, and p/q is an irreducible fraction. Thus, the electron filling that a charge gap can open is quantized to commensurate cases $n = p/q$.[27–29] This condition can also be derived from the generalized Lieb-Schultz-Mattis theorem.[29,30] In this paper, we consider $q = 1$ (half-filling) and $q = 2$ (quarter-filling) cases. At half-filling, in the weak-coupling limit, the couplings of the backward and the Umklapp scattering for the EHM are identified as $g_{1\perp} = -g_{3\perp} = U - 2V$ (see Appendix A).

In addition to the $g_{3\perp}$ term, there exists another Umklapp operator with coupling constant $g_{3\parallel}$, which transfers finite spin.[4,12,28] In the weak-coupling limit, this parameter is identified as $g_{3\parallel} = -2V$. In the present analysis, we will not consider this term explicitly, because the scaling dimension of this term is always higher than that of the other nonlinear terms in Eq. (6). However, in the strong-coupling region, a charge-spin coupling effect may appear due to this term.

If these nonlinear terms are absent ($g_{1\perp} = g_{3\perp} = g_{3\parallel} = 0$), the excitation spectra and their wave numbers in the finite-size system are described by

$$E - E_0 = \frac{2\pi v_\rho}{L} x_\rho + \frac{2\pi v_\sigma}{L} x_\sigma, \quad (7)$$

$$P - P_0 = \frac{2\pi}{L}(s_\rho + s_\sigma) + 2m_\rho k_F, \tag{8}$$

where the scaling dimensions and the conformal spins are given by

$$x_\nu = \frac{1}{2}\left(\frac{n_\nu^2}{K_\nu} + m_\nu^2 K_\nu\right) + N_\nu + \bar{N}_\nu, \tag{9}$$

$$s_\nu = n_\nu m_\nu + N_\nu - \bar{N}_\nu. \tag{10}$$

Here n_ρ is the change of $2n_\rho$ electrons, and n_σ is the total z spins $S_T^z = n_\sigma$. m_ρ (m_σ) denotes the number of particles moved from the left charge (spin) Fermi point to the right one. The non-negative integers N_ν and $\bar{N}_\nu$ are the particle-hole excitations near the right and the left Fermi points, respectively. The scaling dimensions are related to the critical exponents for the correlation functions in the large distance as

$$\langle \mathcal{O}_i(r)\mathcal{O}_i(r')\rangle \propto |r - r'|^{-2(x_{\rho i} + x_{\sigma i})}, \tag{11}$$

where the operator is given by

$$\mathcal{O}_i \equiv \mathcal{O}_{n_\rho,m_\rho}^\rho \mathcal{O}_{n_\sigma,m_\sigma}^\sigma,$$

$$\mathcal{O}_{n_\nu,m_\nu}^\nu \equiv e^{i\sqrt{2}(n_\nu\theta_\nu + m_\nu\phi_\nu)}, \tag{12}$$

or linear combinations of these operators. Therefore, there are one-to-one correspondences between the excitation spectra and the operators.

Now we turn our attention to the excitation spectra, which correspond to the following operators:

$$\mathcal{O}_{\nu 0} \equiv -\frac{4}{K_\nu}\bar{\partial}\phi_\nu\partial\phi_\nu, \tag{13a}$$

$$\mathcal{O}_{\nu 1} \equiv \sqrt{2}\cos(q\sqrt{2}\phi_\nu) \propto \mathcal{O}_{0,q}^\nu + \mathcal{O}_{0,-q}^\nu, \tag{13b}$$

$$\mathcal{O}_{\nu 2} \equiv \sqrt{2}\sin(q\sqrt{2}\phi_\nu) \propto \mathcal{O}_{0,q}^\nu - \mathcal{O}_{0,-q}^\nu, \tag{13c}$$

$$\mathcal{O}_{\nu 3} \equiv \exp(i\sqrt{2}\theta_\nu) = \mathcal{O}_{1,0}^\nu, \tag{13d}$$

where $\mathcal{O}_{\nu 0}$ is the ''marginal field,''[41] and the derivatives are defined by $\partial, \bar{\partial} \equiv (v_\nu^{-1}\partial_\tau \mp i\partial_x)/2$ with imaginary time τ. This operator corresponds to particle-hole excitations near the right and the left Fermi points ($N_\nu = \bar{N}_\nu = 1$). $\mathcal{O}_{\nu 1}$ and $\mathcal{O}_{\nu 2}$ are linear combinations of current excitations ($m_\nu = \pm q$). $\mathcal{O}_{\nu 3}$ is an excitation accompanying variation of the number of electrons or spins ($n_\nu = \pm 1$). We have to choose antiperiodic boundary conditions $\psi_{r,s}(x+L) = -\psi_{r,s}(x)$ to extract the excitation spectra for $\mathcal{O}_{\nu 1}$ and $\mathcal{O}_{\nu 2}$ fields, when q is odd, and $\mathcal{O}_{\nu 3}$ field,[34–36] because the phase fields satisfy the following boundary conditions:[38]

$$\phi_\nu(x+L) = \phi_\nu(x) - \sqrt{2}\pi n_\nu, \tag{14a}$$

$$\theta_\nu(x+L) = \theta_\nu(x) + \sqrt{2}\pi m_\nu, \tag{14b}$$

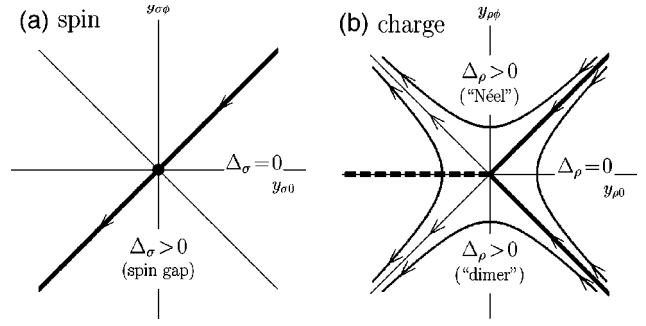and the Fermi operator is given by these phase fields as in Eq. (3).

FIG. 2. RG flow diagram for (a) the spin and (b) the charge degrees of freedom. For the spin sector, the RG flow is fixed on the $y_{\sigma 0} = y_{\sigma \phi}$ line due to the SU(2) symmetry, and the spin-gap transition takes place at $y_{\sigma 0} = y_{\sigma \phi} = 0$. For the charge sector, BKT-type transitions take place on the $y_{\rho 0} = \pm y_{\rho \phi}$ lines with $y_{\rho 0} > 0$. When $q = 1$, the $y_{\rho 0} = +y_{\rho \phi}$ line corresponds to the SU(2) symmetry of the η paring. The $y_{\rho 0} = -y_{\rho \phi}$ line reflects the hidden symmetry of the sine-Gordon model. A Gaussian transition occurs on the $y_{\rho \phi} = 0$ line with $y_{\rho 0} < 0$.

The effects of the $g_{1\perp}$ and the $g_{3\perp}$ terms in Eq. (6) are renormalized in the scaling dimensions x_ν as logarithmic corrections, which are analyzed by the renormalization group (RG) equations derived under the change of the cutoff $\alpha \rightarrow e^{dl}\alpha$ (Ref. 42). Within the one-loop order, the RG equations are given by

$$\frac{dy_{\nu 0}(l)}{dl} = -y_{\nu \phi}^2(l), \tag{15a}$$

$$\frac{dy_{\nu \phi}(l)}{dl} = -y_{\nu 0}(l)y_{\nu \phi}(l), \tag{15b}$$

where $y_{\rho 0}(0) = 2(q^2 K_\rho - 1)$, $y_{\sigma 0}(0) = 2(K_\sigma - 1)$, $y_{\rho \phi}(0) = g_{3\perp}/\pi v_\rho$, $y_{\sigma \phi}(0) = g_{1\perp}/\pi v_\sigma$, and we have set $l = \ln L$. These equations determine the RG flow diagrams. Note that there is a difference between the cases for the charge and the spin sectors reflecting their symmetries (see Fig. 2). In the following subsections, we discuss the phase transitions for each sector described by these RG flow diagrams.

A. Spin-gap transition

First, we consider the phase transition in the spin degree of freedom ($\nu = \sigma$). The spin sector with an SU(2) symmetry belongs to the universality class of the level-1 SU(2) Wess-Zumino-Novikov-Witten (WZNW) model.[43] In this case, the RG flow in Fig. 2(a) is fixed on the $y_{\sigma 0}(l) = y_{\sigma \phi}(l)$ line. Then for $y_{\sigma 0}(l) > 0$, the exponent is renormalized as $K_\sigma^* = 1$, and the solution of Eq. (15) is obtained as

$$y_{\sigma 0}(l) = \frac{y_{\sigma 0}(0)}{y_{\sigma 0}(0)l + 1}, \tag{16}$$

where $y_{\sigma 0}(0)$ is the bare coupling constant. Combining the renormalized coupling and the operator-product-expansion coefficients, the singlet ($x_{\sigma 1}$) and the triplet ($x_{\sigma 2,3}$) excitation spectra split as[44,45,31]

$$x_{\sigma 1}(l) = \frac{1}{2} + \frac{3}{4}y_{\sigma 0}(l), \tag{17a}$$

TABLE I. Correspondence between the g-ology and the level-crossing approach at half-filling. The scaling dimensions $x_{\nu i}$ correspond to excitation spectra of singlet ($x_{\sigma 1}$), triplet ($x_{\sigma 2,3}$), ''dimer'' ($x_{\rho 1}$), ''Néel'' ($x_{\rho 2}$), and ''doublet'' ($x_{\rho 3}$) states. Examples of these level crossings are shown in Figs. 5 and 6.

	g-ology	Level crossing
Spin gap	$g_{1\perp}(=g_\sigma)=0$	$x_{\sigma 1}=x_{\sigma 2,3}$
SU(2)BKT	$g_{3\perp}=g_\rho>0$	$x_{\rho 2}=x_{\rho 3}<x_{\rho 1}$
Hidden SU(2)BKT	$g_{3\perp}=-g_\rho<0$	$x_{\rho 1}=x_{\rho 3}<x_{\rho 2}$
Gaussian	$g_{3\perp}=0, g_\rho<0$	$x_{\rho 1}=x_{\rho 2}<x_{\rho 3}$

$$x_{\sigma 2,3}(l)=\frac{1}{2}-\frac{1}{4}y_{\sigma 0}(l). \qquad (17b)$$

When $y_{\sigma 0}(0)<0$, $y_{\sigma 0}(l)$ is renormalized as $y_{\sigma 0}(l\rightarrow\infty)=-\infty$, then a spin gap appears. At the critical point [$y_{\sigma 0}(0)=0$], there are no logarithmic corrections in the excitation spectra. Therefore, the critical point is obtained by the intersection of the singlet and the triplet excitation spectra ($x_{\sigma 1}=x_{\sigma 2,3}$).[31,34–36] This level crossing corresponds to the condition for the spin-gap phase boundary $g_{1\perp}=g_\sigma=0$ in the standard g-ology analysis, (see Appendix A and Table I).

The asymptotic behavior of the spin gap against a parameter of a model λ near the critical point λ_c is obtained by the two-loop RG equation and the definition of correlation length $y_{\sigma 0}(\ln\xi)\sim-1$ as[34,36]

$$\Delta_\sigma\sim v_\sigma/\xi\propto\sqrt{\lambda-\lambda_c}\exp[-\text{const}/(\lambda-\lambda_c)], \qquad (18)$$

where we have used a relation $\lambda-\lambda_c\propto|y_{\sigma 0}(0)|$. Note that this is the same behavior as that of the spin gap in the 1D negative-U Hubbard model at half-filling.[46]

B. Berezinskii-Kosterlitz-Thouless transition

1. SU(2) symmetric case

Next, we consider the instabilities in the charge sector ($\nu=\rho$), which are described by the RG flow diagram given in Fig. 2(b). At half-filling ($q=1$) and $V=0$ (the Hubbard model), the sign of the on-site interaction U in the Hamiltonian (1) is reversed by the following canonical transformation:[47]

$$c_{j\uparrow}\rightarrow c_{j\uparrow}, \quad c_{j\downarrow}\rightarrow(-1)^j c_{j\downarrow}^\dagger. \qquad (19)$$

This transformation also projects the spin (ζ-pairing) operators onto the η-pairing ones

$$\eta_i^+=(-1)^i c_{i\uparrow}^\dagger c_{i\downarrow}^\dagger, \quad \eta_i^-=(-1)^i c_{i\downarrow}c_{i\uparrow}, \quad \eta_i^z=\frac{1}{2}(n_i-1), \qquad (20)$$

without losing the SU(2) symmetry.[48] It follows from Eq. (3) this transformation corresponds to the replacement of the indices as $\rho\leftrightarrow\sigma$. Therefore, the spin part of the sine-Gordon model of Eq. (6) is mapped onto the charge part, and the operators $\mathcal{O}_{\rho 1}$ and $\mathcal{O}_{\rho 2}$, $\mathcal{O}_{\rho 3}$ denote the ''singlet'' and the ''triplet'' for the charge part, respectively. Thus, the exponent is renormalized as $K_\rho^*=1$ for $U<0$, and the charge gap opens for $U>0$.

In the case when the SU(2) symmetry in the charge sector is broken by finite V, $\mathcal{O}_{\rho 1}$, $\mathcal{O}_{\rho 2}$, and $\mathcal{O}_{\rho 3}$ refer to ''dimer,'' ''Néel,'' and ''doublet,'' respectively, by following Ref. 32. Then, if the initial value of the RG flow moves across the SU(2)-symmetric line [$y_{\rho\phi}(0)=y_{\rho 0}(0)>0$], a Berezinskii-Kosterlitz-Thouless (BKT)-type transition[49,50,42] occurs between the TL liquid phase and the twofold-degenerate gapped state. For this transition, one can show that a charge gap opens as[42]

$$\Delta_\rho\propto\exp(-\text{const}/\sqrt{\lambda-\lambda_c}), \qquad (21)$$

where $|\lambda-\lambda_c|\propto t$, and $t\equiv|y_{\rho\phi}(l)|/y_{\rho 0}(l)-1$ stands for the deviation from the BKT critical line. Note that Eq. (21) is a different asymptotic behavior from that of the spin-gap transition described by Eq. (18), so that we discriminate the spin-gap transition from BKT-type transitions in this paper. The critical point for this BKT transition can be obtained without calculations, because it is fixed by the SU(2) symmetry of the Hamiltonian. In the case of the EHM, the BKT transition line is fixed on the $V=0$ line for $U<0$.

Now, we consider the region for $y_{\rho\phi}(l)<0$. The sine-Gordon model has a symmetry under the transformation to reverse the sign of the nonlinear term $\cos\sqrt{8}\phi_\rho$. This transformation corresponds to the shift of the phase fields:

$$\phi_\rho\rightarrow\phi_\rho+\pi/\sqrt{8}. \qquad (22)$$

This operation interchanges the roles of the operators $\mathcal{O}_{\rho 1}$ and $\mathcal{O}_{\rho 2}$ as

$$\cos\sqrt{2}\phi_\rho\rightarrow-\sin\sqrt{2}\phi_\rho, \qquad (23a)$$

$$\sin\sqrt{2}\phi_\rho\rightarrow\cos\sqrt{2}\phi_\rho. \qquad (23b)$$

Therefore, this symmetry indicates that the SU(2)-symmetric line in the RG flow diagram is mapped onto the opposite side of the $y_{\rho 0}$ axis, and another BKT transition may occur at $y_{\rho\phi}(0)=-y_{\rho 0}(0)<0$. We call the symmetry of this BKT line ''hidden SU(2) symmetry.'' Since this symmetry originates from that of the sine-Gordon model, it is not contained explicitly in the original Hamiltonian. The renormalized scaling dimensions of $\mathcal{O}_{\rho 1}$, $\mathcal{O}_{\rho 2}$, and $\mathcal{O}_{\rho 3}$ near the critical line of the hidden SU(2) symmetry are calculated as follows:[45,32]

$$x_{\rho 1}(l)=\frac{1}{2}-\frac{1}{4}y_{\rho 0}(l)(1+2t), \qquad (24a)$$

$$x_{\rho 2}(l)=\frac{1}{2}+\frac{3}{4}y_{\rho 0}(l)\left(1+\frac{2}{3}t\right), \qquad (24b)$$

$$x_{\rho 3}(l)=\frac{1}{2}-\frac{1}{4}y_{\rho 0}(l). \qquad (24c)$$

Therefore, the critical point for the hidden SU(2) BKT transition can be determined by the level crossing between the ''dimer'' and the ''doublet'' excitation spectra ($x_{\rho 1}=x_{\rho 3}<x_{\rho 2}$).[32] This level crossing corresponds to the condition $g_{3\perp}=-g_\rho<0$ in the g-ology analysis (see Appendix A and Table I).

2. Non-SU(2) symmetric case

We consider the BKT transition for $q \geq 2$ case. This situation may appear in the metal-insulator transition at quarter-filling ($q = 2$). In this case, the critical line no longer has an SU(2) symmetry. However, by replacing the variables as $\phi'_\rho = q\phi_\rho$, $\theta'_\rho = \theta_\rho/q$, and $K'_\rho = q^2 K_\rho$, the sine-Gordon model for the charge part of Eq. (6) is mapped onto the case of $q = 1$. Then, the BKT transition between the TL liquid and the $2q$-fold-degenerate gapped state takes place when the renormalized exponent becomes $K^*_\rho = 1/q^2$. The scaling dimensions for the $\mathcal{O}_{\rho 1}$ and the $\mathcal{O}_{\rho 2}$ fields near the BKT critical line remain unchanged, while the $\mathcal{O}_{\rho 3}$ field changes as

$$x_{\rho 3}(l) = q^2 \left[\frac{1}{2} - \frac{1}{4} y_{\rho 0}(l) \right]. \tag{25}$$

Therefore, the BKT critical point corresponding to $y_{\rho\phi} = y_{\rho 0} > 0$ is given by the level-crossing point of $x_{\rho 2} = x_{\rho 3}/q^2 < x_{\rho 1}$.

There is another excitation spectrum that can be used to determine the BKT critical point. This is the ''marginal field'' (13a) whose renormalized scaling dimension is given by[33]

$$x_{\rho 0}(l) = 2 - y_{\rho 0}(l)\left(1 + \frac{4}{3}t\right). \tag{26}$$

In this case, the critical point can be determined by the level crossing of $x_{\rho 0} = 4x_{\rho 2}$.

C. Gaussian transition

In addition to these BKT-type transitions, a Gaussian transition occurs at $y_{\rho\phi}(0) = 0$ and $y_{\rho 0}(0) < 0$. This is a second-order transition between the two gapped states, which corresponds to the different fixed points $[y_{\rho\phi}(l \to \infty) = \pm\infty]$, and the gap vanishes just on the critical point. The transition point is given by the level crossing between the ''dimer'' and the ''Néel'' excitations ($x_{\rho 1} = x_{\rho 2} < x_{\rho 3}$), because the $\mathcal{O}_{\rho 1}$ and the $\mathcal{O}_{\rho 2}$ fields interchange their roles at $y_{\rho\phi}(0) = 0$ as was explained in Sec. II B 1. In the g-ology, this level crossing corresponds to the condition $g_{3\perp} = 0$ with $g_\rho < 0$ (see Appendix A and Table I). Since the nonlinear term vanishes on the critical line, there is no effect of the renormalization. Therefore, the scaling dimensions on the Gaussian line are given by

$$x_{\rho 1} = x_{\rho 2} = \frac{K_\rho}{2}, \tag{27a}$$

$$x_{\rho 3} = \frac{1}{2K_\rho}, \tag{27b}$$

without logarithmic corrections, and $K_\rho < 1$ is satisfied. The asymptotic form of the gap near the Gaussian transition point can be obtained by solving Eq. (15b) with an approximation $y_{\rho 0}(l) \approx y_{\rho 0}(0)$ and definition of the correlation length $|y_{\rho\phi}(\ln \xi)| \sim 1$ as[32]

$$\Delta_\rho \sim v_\rho/\xi \propto |\lambda - \lambda_c|^{[1/2(1-K_\rho)]}, \tag{28}$$

where we have used the relation $y_{\rho\phi}(0) \propto \lambda - \lambda_c$. The valley of the gap becomes steeper as K_ρ is decreased.

III. DISCRETE SYMMETRIES

To perform the level-crossing analysis discussed in Sec. II, we need to identify the relevant excitation spectra. For this purpose, we discuss the discrete symmetries of wave functions corresponding to the excited states. The physical meaning of these symmetries will be clarified in Sec. IV.

The discrete symmetries are defined under particle-hole $[\mathcal{C}: c_{is} \to (-1)^i c^\dagger_{is}]$, space-inversion ($\mathcal{P}: c_{is} \to c_{L-i+1,s}$), and spin-reversal ($\mathcal{T}: c_{is} \to c_{i,-s}$) transformations. They give eigenvalues ± 1. In addition, shift operation by one site ($\mathcal{S}: c_{is} \to c_{i+1,s}$) is defined, which has an eigenvalue e^{ik}. The symmetries of wave functions can be explained by combining those of the ground state and those of the operators for the excited states.[36] For the ground state of the EHM, we choose periodic (antiperiodic) boundary conditions when $N/2$ is odd (even), where N is the number of electrons. Then, according to the Perron-Frobenious theorem, the discrete symmetries of the ground state are $\mathcal{C} = \mathcal{P} = \mathcal{T} = 1$ and $k = 0$, if we choose the representation for the basis and use the symmetry operations defined in Ref. 36.

Next, we consider the symmetries of operators. The operator of the marginal field (13a) has the same quadratic form of the Gaussian part of the Lagrangian density of Eq. (6), so that it has the same symmetry as the ground state ($\mathcal{C} = \mathcal{P} = \mathcal{T} = 1$, $k = 0$). We can find the symmetries of the $\mathcal{O}_{\nu 1}$ and the $\mathcal{O}_{\nu 2}$ operators by considering the change of the phase fields. Since we restrict our attention to the Hilbert space with fixed electron number and total z spin, we do not consider the change of the θ_ν fields in the symmetry operations. At half-filling ($k_F = \pi/2$), it follows from Eq. (3) that the phase fields ϕ_ν are transformed under particle-hole ($\mathcal{C}: \psi_{r,s} \leftrightarrow \psi^\dagger_{r,s}$), space-inversion ($\mathcal{P}:$ R$\leftrightarrow$L, $x \to x+a$), spin-reversal transformations ($\mathcal{T}: \uparrow \leftrightarrow \downarrow$), and shift operation ($\mathcal{S}: x \to x+a$) as

$$\mathcal{C}: \phi_\sigma \to -\phi_\sigma, \quad \phi_\rho \to -\phi_\rho, \tag{29a}$$

$$\mathcal{P}: \phi_\sigma \to -\phi_\sigma, \quad \phi_\rho \to -\phi_\rho, \tag{29b}$$

$$\mathcal{T}: \phi_\sigma \to -\phi_\sigma, \quad \phi_\rho \to \phi_\rho, \tag{29c}$$

$$\mathcal{S}: \phi_\sigma \to \phi_\sigma, \quad \phi_\rho \to \sqrt{2}k_F + \phi_\rho. \tag{29d}$$

In this case, $\mathcal{CP} = 1$ is always satisfied, so that the independent discrete symmetries are $\mathcal{P}$, $\mathcal{T}$, and $\mathcal{S}$. At quarter-filling ($k_F = \pi/4$), the phase fields change as

$$\mathcal{P}: \phi_\sigma \to -\phi_\sigma, \quad \phi_\rho \to \pi/\sqrt{8} - \phi_\rho. \tag{30}$$

Thus the discrete symmetries of the operator $\mathcal{O}_{\rho 1}$ for $q = 2$ are $\mathcal{P} = -1$. The relations between the operators and their symmetries are summarized in Table II.

In the present numerical calculation based on the Lanczös algorithm, the identification is performed by projecting the initial vector as

$$|\Psi_{init}\rangle = \frac{1}{2}(1 \pm \mathcal{P})(1 \pm \mathcal{T})|i\rangle, \tag{31}$$

TABLE II. Discrete symmetries of the excitation spectra ($\mathcal{C}$: charge conjugation, $\mathcal{P}$: space inversion, $\mathcal{T}$: spin reversal, and k: wave number). BC$=1$ (BC$=-1$) stands for (anti)periodic boundary conditions. The upper (lower) sign of BC denotes $N/2=$ odd (even) cases, where N is the number of electrons. The upper 12 states are "physical" ones, which appear under the same BC as those of the ground state. The lower six states are the "artificial" ones extracted by twisting BC with respect to the ground state.

	Operators	$\mathcal{C}$	$\mathcal{P}$	$\mathcal{T}$	k	BC
Ground state	1	1	1	1	0	± 1
Marginal	$-4K_\nu^{-1}\bar\partial\phi_\nu\partial\phi_\nu$	1	1	1	0	± 1
CDW	$\sin\sqrt{2}\phi_\rho\cos\sqrt{2}\phi_\sigma$	-1	-1	1	$2k_F$	± 1
SDW$_z$	$\cos\sqrt{2}\phi_\rho\sin\sqrt{2}\phi_\sigma$	-1	-1	-1	$2k_F$	± 1
SDW$_\pm$	$\cos\sqrt{2}\phi_\rho\exp\pm i\sqrt{2}\theta_\sigma$	$*$	1	$*$	$2k_F$	± 1
BCDW	$\cos\sqrt{2}\phi_\rho\cos\sqrt{2}\phi_\sigma$	1	1	1	$2k_F$	± 1
BSDW$_z$	$\sin\sqrt{2}\phi_\rho\sin\sqrt{2}\phi_\sigma$	1	1	-1	$2k_F$	± 1
BSDW$_\pm$	$\sin\sqrt{2}\phi_\rho\exp\pm i\sqrt{2}\theta_\sigma$	$*$	-1	$*$	$2k_F$	± 1
SS	$\exp i\sqrt{2}\theta_\rho\cos\sqrt{2}\phi_\sigma$	$*$	1	1	0	± 1
TS$_0$	$\exp i\sqrt{2}\theta_\rho\sin\sqrt{2}\phi_\sigma$	$*$	-1	-1	0	± 1
TS$_{\pm 1}$	$\exp i\sqrt{2}\theta_\rho\exp\pm i\sqrt{2}\theta_\sigma$	$*$	1	$*$	0	± 1
$4k_F$-CDW	$\cos 2\sqrt{2}\phi_\rho$	$*$	-1	$*$	$4k_F$	± 1
singlet	$\cos\sqrt{2}\phi_\sigma$	1	1	1	0	∓ 1
triplet$_0$	$\sin\sqrt{2}\phi_\sigma$	-1	-1	-1	0	∓ 1
triplet$_{\pm 1}$	$\exp\pm i\sqrt{2}\theta_\sigma$	$*$	1	$*$	0	∓ 1
"dimer"	$\cos\sqrt{2}\phi_\rho$	1	1	$*$	$2k_F$	∓ 1
"Néel"	$\sin\sqrt{2}\phi_\rho$	-1	-1	$*$	$2k_F$	∓ 1
"doublet"	$\exp\pm i\sqrt{2}\theta_\rho$	$*$	1	1	0	∓ 1

where the signs in front of the operators correspond to their eigenvalues, and $|i\rangle$ is a configuration that satisfies $\mathcal{P},\mathcal{T}|i\rangle \neq |i\rangle$. Furthermore, $|i\rangle$ is classified by the wave numbers $k=0,\pi$.

IV. PHASES

In this section, we discuss the character of each phase that appears in the phase diagrams. In general, there are no long-range orders (LRO's) in 1D systems due to strong quantum fluctuations, so that, in such cases, the phases are characterized by the dominant correlation functions. The correlation functions (11) including the logarithmic corrections are given by integrating the renormalized scaling dimensions over the RG trajectory as

$$R_i = \exp\left[-\int_0^{\ln(r/\alpha)} dl\, 2[x_{\rho i}(l)+x_{\sigma i}(l)]\right]. \quad (32)$$

First, we consider Eq. (32) for the spin and charge degrees of freedom independently. For the spin part which has the SU(2) symmetry, the singlet ($\mathcal{O}_{\sigma 1}$) and the triplet ($\mathcal{O}_{\sigma 2,3}$) correlation functions with logarithmic corrections are obtained explicitly in the gapless region ($g_{1\perp}^*=0,K_\sigma^*=1$) as[45]

$$R_{\sigma 1}=\frac{\alpha}{r}\ln^{-3/2}(r/\alpha), \quad (33a)$$

$$R_{\sigma 2,3}=\frac{\alpha}{r}\ln^{1/2}(r/\alpha), \quad (33b)$$

where we have used Eqs. (16), (17), and (32). Therefore, the triplet correlation is more logarithmically dominant than the singlet one. On the other hand, when the spin gap opens ($g_{1\perp}^*=-\infty$), the singlet excitation degenerates with the ground state in the thermodynamic limit, so that the singlet correlation becomes constant, while the triplet one decays exponentially. In this way, the triplet correlation is suppressed in the spin-gap region.

For the charge part, at half-filling, explicit forms of the correlation functions including logarithmic corrections are not obtained except for the BKT or the Gaussian lines. On the BKT line, the exponent is renormalized as $K_\rho^*=1$, so that $K_\rho^*\geq 1$ is always satisfied in the gapless region ($g_{3\perp}^*=0$), and then the correlation for the "doublet" ($\mathcal{O}_{\rho 3}$) is dominant. In the charge-gap region with $g_{3\perp}^*=\infty$, the "Néel" ($\mathcal{O}_{\rho 2}$) state degenerates with the ground state, and the "dimer" ($\mathcal{O}_{\rho 1}$) and the "doublet" correlations decay exponentially. On the other hand, for $g_{3\perp}^*=-\infty$, the "dimer" state degenerates with the ground state, and the "Néel" and the "doublet" correlations decay exponentially.

Next, we discuss the physical states that consist of the charge and the spin parts. In the metallic region ($g_{3\perp}^*=0,K_\rho^*\geq 1$), the triplet superconducting (TS) correlation is dominant when the spin part is gapless. The operators for the TS phase consist of the "doublet" and the triplet ones,

$$\mathcal{O}_{TS_0}=\sum_s c_{js}^\dagger c_{j+1,-s}^\dagger,$$

$$\propto \exp[+i\sqrt{2}\theta_\rho(x)]\sin[\sqrt{2}\phi_\sigma(x)], \quad (34a)$$

$$\mathcal{O}_{TS_1}=c_{j\uparrow}^\dagger c_{j+1,\uparrow}^\dagger,$$

$$\propto \exp[+i\sqrt{2}\theta_\rho(x)]\exp[+i\sqrt{2}\theta_\sigma(x)]. \quad (34b)$$

On the other hand, the singlet superconducting (SS) correlation whose operator is given by the "doublet" and the singlet ones

$$\mathcal{O}_{SS}=c_{j\uparrow}^\dagger c_{j\downarrow}^\dagger\propto \exp[+i\sqrt{2}\theta_\rho(x)]\cos[\sqrt{2}\phi_\sigma(x)], \quad (35)$$

is dominant when the spin part has a gap.

In the insulating region, which corresponds to the fixed point $g_{3\perp}^*=+\infty$, the bond-spin-density-wave (BSDW) phase[22] characterized by

$$\mathcal{O}_{BSDW\alpha}=(-1)^j\sum_{s,s'} (c_{js}^\dagger\tau_{ss'}^\alpha c_{j+1,s'}+c_{j+1,s}^\dagger\tau_{ss'}^\alpha c_{js'}),$$

$$\mathcal{O}_{BSDWz}\propto \sin[\sqrt{2}\phi_\rho(x)]\sin[\sqrt{2}\phi_\sigma(x)], \quad (36a)$$

$$\mathcal{O}_{BSDW\pm}\propto \sin[\sqrt{2}\phi_\rho(x)]\exp[\pm i\sqrt{2}\theta_\sigma(x)], \quad (36b)$$

appears when the spin sector is gapless. On the other hand, the charge-density-wave (CDW) phase

$$\mathcal{O}_{CDW}=(-1)^j\sum_s c_{js}^\dagger c_{js}\propto \sin[\sqrt{2}\phi_\rho(x)]\cos[\sqrt{2}\phi_\sigma(x)], \quad (37)$$

TABLE III. Correspondence between six possible phases at half-filling and fixed points in the RG analysis. For $g_{1\perp}^* = -\infty$ ($g_{1\perp}^* = 0$), the spin sector is gapped (gapless). For $g_{3\perp}^* = \pm\infty$ ($g_{3\perp}^* = 0$), the charge sector is gapped (gapless).

	$g_{3\perp}^* = 0$	$g_{3\perp}^* = +\infty$	$g_{3\perp}^* = -\infty$
$g_{1\perp}^* = 0$	TS	BSDW	SDW
$g_{1\perp}^* = -\infty$	SS	CDW (LRO)	BCDW (LRO)

appears when the spin gap opens. In the CDW phase, both charge and spin gaps open, so that a LRO exists.

In the insulating region for the opposite fixed point $g_{3\perp}^* = -\infty$, the spin-density-wave (SDW) correlation characterized by

$$\mathcal{O}_{SDW\alpha} = (-1)^j \sum_{s,s'} c_{js}^\dagger \tau_{ss'}^\alpha c_{js'},$$

$$\mathcal{O}_{SDW_z} \propto \cos[\sqrt{2}\phi_\rho(x)]\sin[\sqrt{2}\phi_\sigma(x)], \qquad (38a)$$

$$\mathcal{O}_{SDW_\pm} \propto \cos[\sqrt{2}\phi_\rho(x)]\exp[\pm i\sqrt{2}\theta_\sigma(x)], \qquad (38b)$$

is dominant when the spin part is gapless. The bond-charge-density-wave (BCDW) phase characterized by

$$\mathcal{O}_{BCDW} = (-1)^j \sum_s (c_{js}^\dagger c_{j+1,s} + c_{j+1,s}^\dagger c_{js}),$$

$$\propto \cos[\sqrt{2}\phi_\rho(x)]\cos[\sqrt{2}\phi_\sigma(x)], \qquad (39)$$

appears when the spin gap opens. In the BCDW phase, both charge and spin gaps open, so that a LRO exists. The correspondence between the above six phases at half-filling and the fixed points are summarized in Table III.

At quarter-filling ($q=2$), the $4k_F$-charge-density wave ($4k_F$-CDW) appears when the Umklapp scattering is relevant. The operator is given by the $\mathcal{O}_{\rho 1}$ field with $q=2$,

$$\mathcal{O}_{4CDW} = \sum_r \psi_{r\uparrow}^\dagger(x)\psi_{r\downarrow}^\dagger(x)\psi_{-r\downarrow}(x)\psi_{-r\uparrow}(x),$$

$$\propto \cos[\sqrt{8}\phi_\rho(x)]. \qquad (40)$$

In the rest of this section, we further clarify the differences among the four charge-gapped states (CDW, SDW, BCDW, and BSDW) discussed above. For this purpose, we change the basis of the bosonized operators from the charge and spin picture to the spin up and down one by introducing the following new phase fields:

$$\phi_s = \phi_\rho \pm \phi_\sigma, \qquad (41)$$

where $s = \uparrow, \downarrow$ refer to the upper and lower signs, respectively. Then, the system is interpreted as coupled spinless fermion systems ($S=1/2$ spin chains). In this case, the (B)CDW and z-components of the (B)SDW operators are given by

$$\mathcal{O}_{CDW}, \mathcal{O}_{SDW_z} \propto \sin(\sqrt{2}\phi_\downarrow) \pm \sin(\sqrt{2}\phi_\uparrow), \qquad (42)$$

$$\mathcal{O}_{BCDW}, \mathcal{O}_{BSDW_z} \propto \cos(\sqrt{2}\phi_\uparrow) \pm \cos(\sqrt{2}\phi_\downarrow), \qquad (43)$$
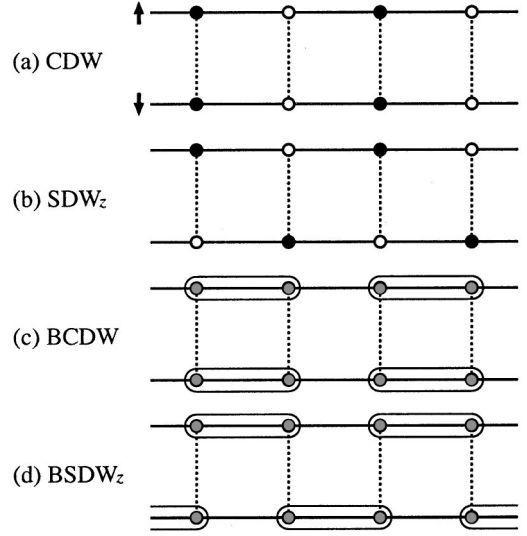

FIG. 3. Schematic illustration for the four charge-gapped states in up and down spin subsystems. The enclosed two sites in (c) and (d) stand for electron-hole dimers. The electrons polarize on sites ($\mathcal{C} = \mathcal{P} = -1$) for CDW and SDW states, while they polarize on bonds ($\mathcal{C} = \mathcal{P} = +1$) for BCDW and BSDW states. The two subsystems are synchronized ($\mathcal{T} = +1$) for CDW and BCDW states, while they are displaced by one site ($\mathcal{T} = -1$) for SDW and BSDW states.

where the CDW and the BCDW (the SDW_z and the $BSDW_z$) operators refer to the upper (lower) signs in the right-hand sides, and $\sin(\sqrt{2}\phi_s)$ and $\cos(\sqrt{2}\phi_s)$ fields denote Néel and dimer states of the $S=1/2$ spin chains, respectively. In addition, it follows from Eqs. (29d) and (41) that the shift operation by one site gives

$$\phi_s \to \phi_s + \pi/\sqrt{2}, \qquad (44)$$

so that both CDW and SDW_z states are described by two Néel ordered spin chains, where the two sectors ($s = \uparrow, \downarrow$) are synchronized in the former, while they are displaced by one site in the latter. On the other hand, the BCDW and the $BSDW_z$ states are given by synchronized and displaced dimer-ordered spin chains, respectively (see Fig. 3). Therefore, in the BCDW phase, the charge is polarized on the bonds alternatively, and the spins are dimerized. In the BSDW state, the charge is polarized on the each bond, and the spins are located on the bonds and remain gapless like the SDW state.[22]

The discrete symmetries discussed in Sec. III characterize the differences among these physical states. It follows from Eq. (29), that the spin reversal symmetry corresponds to whether $s = \uparrow, \downarrow$ sectors are synchronized ($\mathcal{T} = +1$) or displaced by one site ($\mathcal{T} = -1$). Similarly, the parity and the charge conjugation distinguish whether the electrons are polarized on the sites ($\mathcal{C} = \mathcal{P} = -1$) or on the bonds ($\mathcal{C} = \mathcal{P} = +1$). This interpretation for the parity is consistent with the fact that the $4k_F$-CDW with a site LRO has the odd parity ($\mathcal{P} = -1$) at quarter-filling.

V. HALF-FILLING

Using the method explained in Sec. II, we analyze the phase diagram of the EHM at half-filling. Since there are
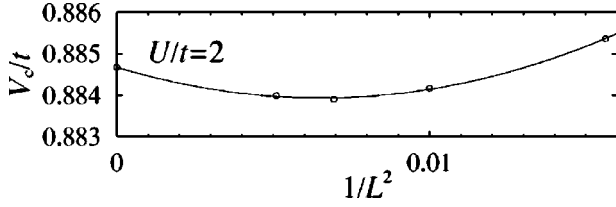
FIG. 4. Size dependence of the critical point for the spin-gap transition at $U/t=2$. The system sizes are $L=8,10,12,14$. From Ref. 16.

many instabilities, we consider the phase diagram separately in the charge and the spin parts by assuming the charge-spin separation. However, for the CDW-SDW transition, there is a possibility that the charge and the spin degrees of freedom are coupled. So we discuss two cases where the two degrees of freedom are separated and coupled. And then we identify the valid scenario from the comparison with the result of the strong-coupling perturbation theory. For the phase separation, which is considered to be a first-order transition, we need an approach different from the one applied to the charge- and the spin-gap phases. We discuss the way to determine the phase-separation boundary and check the validity of the result by the strong-coupling theory. Using the above strategy, we also analyze the EHM with the correlated hopping term [Eq. (2)]. The results are summarized in Fig. 15.

A. Spin sector

First, we determine the spin-gap phase boundary following the method explained in Sec. II A. By observing the singlet-triplet level crossing, the phase boundary is found to be near the $U=2V$ line. Since the critical point is almost independent of the system size (see Fig. 4), we can determine the phase boundary without any extrapolations. In order to check the consistency of our argument, we calculate scaling dimensions of the singlet and the triplet excitations from Eq. (7), and confirm the ratios of the logarithmic corrections. Here the spin-wave velocity is given by the excitation spectra for $N_\sigma(\bar{N}_\sigma)=1$ or $|n_\sigma|=|m_\sigma|=1$ as
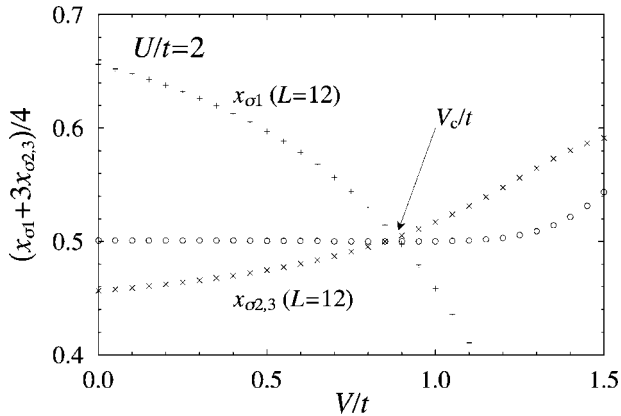

FIG. 5. Extrapolated scaling dimension given by Eq. (46) near the spin-gap critical point at $U/t=2$. The TL liquid theory predicts the numerical values are 1/2 in the gapless region ($V<V_c$). This result shows the existence of the spin-gap transition. The scaling dimensions for the singlet ($x_{\sigma1}$) and the triplet ($x_{\sigma2,3}$) excitation spectra in the $L=12$ system are also shown.
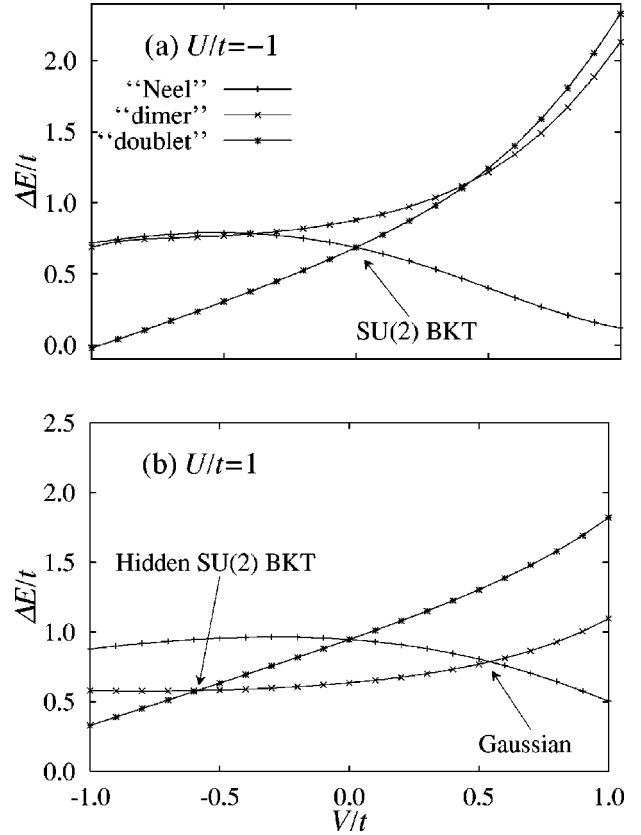

FIG. 6. "Dimer"$(x_{\rho1})$, "Néel"$(x_{\rho2})$, and "doublet"$(x_{\rho3})$ excitation spectra in the charge sector vs V/t in $L=8$ system at (a) $U/t=-1$ and (b) $U/t=1$. In the $U/t<0$ region, a BKT-type transition takes place at $V/t=0$ reflecting the SU(2) symmetry of the η-pairing. In the $U/t>0$ region, two level crossings occur due to the hidden SU(2) symmetric BKT and the Gaussian transitions. These three level crossings give the Y-shaped structure in the phase diagram.

$$v_\sigma = \lim_{L\to\infty} \frac{E(L,N,S=1,k=2\pi/L)-E_0(L,N)}{2\pi/L}, \quad (45)$$

where the extrapolation is performed by the function $v_\sigma(L) = v_\sigma(\infty)+A/L^2+B/L^4$, which is explained by $x_\nu=4$ irrelevant fields.[51,52] Physically, this correction is related to the deviation from the linearized dispersion relation assumed in the TL model. Thus, the ratio of the logarithmic corrections can be checked as $3:-1$ for the singlet and the triplet states by using the following relation near the critical point,

$$\frac{x_{\sigma1}+3x_{\sigma2,3}}{4}=\frac{1}{2}. \quad (46)$$

Here we use the numerical data of $L=8,10,12$ systems to check the scaling dimensions, and extrapolate them by the form $A+BL^{-2}+CL^{-4}$ as in the same way of the spin velocity. As shown in Fig. 5, the extrapolated data become 1/2 in the gapless region. Thus, the universality of the transition is identified as the level-1 SU(2) WZNW model.

B. Charge sector

Due to the SU(2) symmetry of the η-pairing (20), a BKT transition takes place on the $V=0$ line for the $U<0$ region.
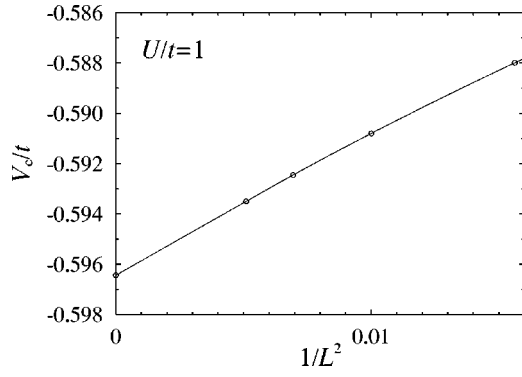
FIG. 7. Size dependence of the critical point of the BKT transition due to the hidden SU(2) symmetry at $U/t=1$. The system sizes are $L=8,10,12,14$.

This phase boundary is fixed on this line for any strength of $U<0$. In Fig. 6(a), the degeneracy of the ''Néel'' ($x_{\rho 2}$) and the ''doublet'' ($x_{\rho 3}$) excitation spectra on $V=0$ corresponds to this SU(2) symmetry. On the other hand, for the $U>0$ region, there appear two relevant level crossings as shown in Fig. 6(b). The one corresponds to the BKT transition due to the hidden SU(2) symmetry, and the other corresponds to the Gaussian transition, as was explained in Sec. II. The rest of the three level crossings in Fig. 6 do not correspond to any phase transitions, because they correspond to the lines $\pm y_{\rho\phi}(0)=y_{\rho 0}(0)<0$ and the line $y_{\rho\phi}(0)=0$ with $y_{\rho 0}(0)>0$ (Gaussian fixed line), in the RG flow diagram of Fig. 2(b).

The hidden SU(2) BKT transition obtained by the ''dimer''-''doublet'' level crossing ($x_{\rho 1}=x_{\rho 3}$) appears near the $U=-2V$ line as was predicted by the g-ology. The size dependence of this transition at $U/t=1$ is shown in Fig. 7. In order to check the consistency of our argument, we calculate the scaling dimensions of $x_{\rho i}$ using Eq. (7). Here, we calculate the charge velocity using the excitation spectra for $N_\rho(\bar{N}_\rho)=1$ as

$$v_\rho = \lim_{L\to\infty} \frac{E(L,N,S=0,k=2\pi/L)-E_0(L,N)}{2\pi/L}. \quad (47)$$

Using Eqs. (24), we check the following relation on the critical line,

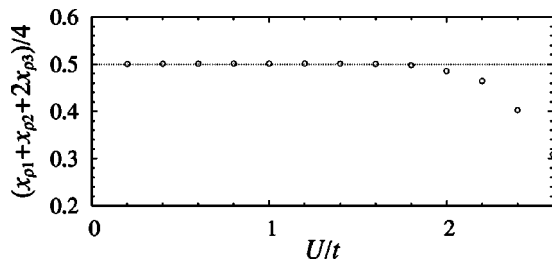$$\frac{x_{\rho 1}+x_{\rho 2}+2x_{\rho 3}}{4}=\frac{1}{2}. \quad (48)$$

FIG. 8. Extrapolated scaling dimension given by Eq. (48) on the BKT critical line. The TL liquid theory predicts the numerical values are 1/2. This result shows the existence of the BKT-type transition.
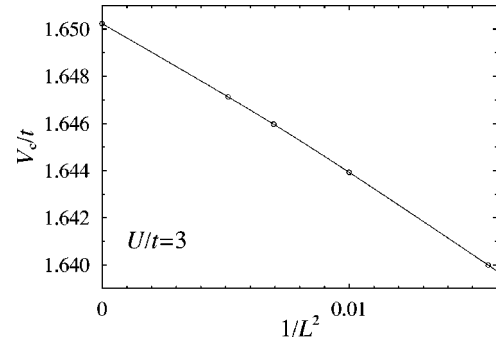

FIG. 9. Size dependence of the critical point for the Gaussian transition at $U/t=3$. The system sizes are $L=8,10,12,14$. The data agrees with the result of Cannon et $al.$[13] that $V_c/t=1.65^{+0.10}_{-0.05}$, from Ref. 16.

As shown in Fig. 8, the extrapolated data become 1/2. Here, the extrapolation is performed as in the same way of the spin-gap transition. Thus, the universality class of this transition is identified as a BKT type. The deviation from the expected value 1/2 in Fig. 8 stands for the effect of the phase separation where the TL liquid theory breaks down.

The Gaussian transition takes place along the $U=2V$ line as was predicted by the g-ology. The size dependence of this transition at $U/t=3$ is shown in Fig. 9. It follows from Eq. (27), the following relation should be satisfied just on the Gaussian transition line,

$$\frac{x_{\rho 1}+x_{\rho 2}}{2}x_{\rho 3}=\frac{1}{4}. \quad (49)$$

The result is shown in Fig. 10. The extrapolated data become 1/4 from the weak- to the intermediate-coupling region. Thus, the transition is identified as a Gaussian type except for the strong-coupling region.

C. Transition between CDW and SDW phases

We have determined the spin-gap and Gaussian transition lines near the $U=2V$ line assuming the charge-spin separation, however, if the $g_{3\parallel}$ term in Eq. (6) is relevant, the charge-spin coupling may take place. Therefore, we should consider the possibility that the charge and the spin degrees of freedom are not separated, and that a direct transition between the CDW and the SDW phases takes place. To examine this possibility, we also observe the level crossing of excitation spectra of the CDW and the SDW operators (see
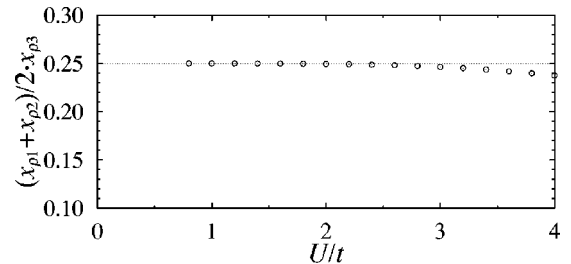

FIG. 10. Extrapolated scaling dimension given by Eq. (49) on the Gaussian critical line. The TL liquid theory predicts the numerical values are 1/4. This result shows the existence of the Gaussian transition.
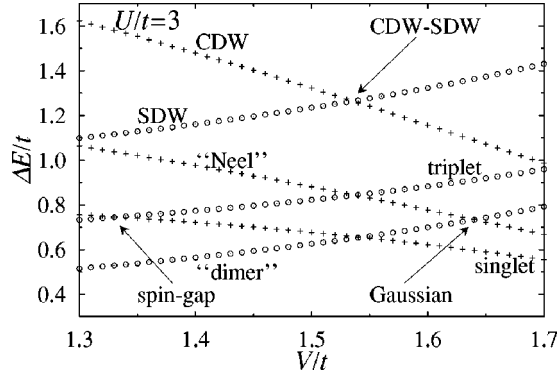
FIG. 11. Six excitation spectra vs V/t in $L=8$ system at $U/t=3$ near the $U=2V$ line.

Table II), which consist of both charge and spin components. These spectra can be obtained under conditions given in Table II.

The level-crossing points for the three assumed transition lines are close to the $U=2V$ line, but slightly deviate (see Fig. 11). The deviations from $U=0$ to $U=\infty$ are shown in Fig. 12. These three lines coincide in the weak- and the strong-coupling limits. For the Gaussian line, the finite-size effect is small for all regions. For the spin-gap phase boundary, the finite-size effect is small in the weak-coupling region, but it becomes large in the strong-coupling region. The direct CDW-SDW level-crossing point has large size effect for all regions.

In order to identify the actual transition lines from these three lines, we use the strong-coupling perturbation theory following Hirsch[6] and van Dongen.[7] The energy of the SDW state in the strong-coupling region of the EHM are analytically obtained up to the fourth order. If we include the correlated hopping term (2) in the EHM, the energies of the CDW and the SDW states are given by
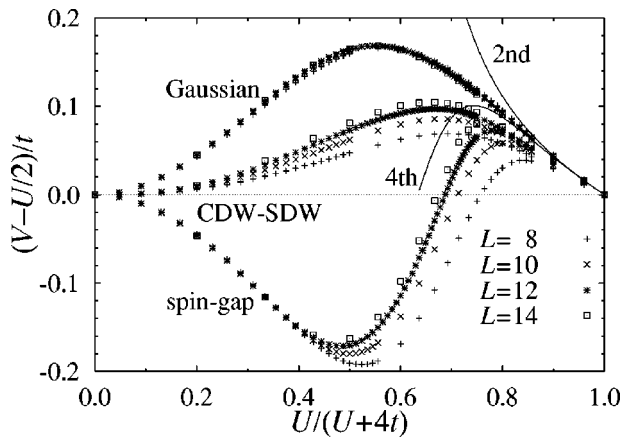

FIG. 12. Three possible transitions (Gaussian, spin-gap, and direct CDW-SDW transitions) along the $U=2V$ line of the EHM calculated in $L=8,10,12,14$ systems. The result of the strong-coupling expansion [Eq. (53) with $\xi=0$] agrees with the Gaussian transition. This means that the actual transitions are the Gaussian and the spin-gap transitions, and a BCDW state exists between them, from Ref. 16.

$$\frac{E_{\mathrm{CDW}}}{L}=\frac{U}{2}-\frac{2(1-\xi)^2 t^2}{(3v-1)U}$$

$$+\frac{(1-\xi)^2[(36v^2-5v-1)(1-\xi)^2-8(3v-1)v]t^4}{v(3v-1)^3(4v-1)U^3},$$

$$(50)$$

$$\frac{E_{\mathrm{SDW}}}{L}=V-\frac{4(1-\xi)^2 t^2\ln 2}{(1-v)U}$$

$$+9\zeta(3)\frac{(1-\xi)^2[2(1-\xi)^2-1+v]t^4}{(1-v)^3 U^3},\quad(51)$$

where $v\equiv V/U$ and $\xi\equiv X/t$. In Eq. (51), we have used the Bethe-ansatz result of the $S=1/2$ Heisenberg spin chain:[53,54]

$$\langle S_i\cdot S_{i+1}\rangle-\frac{1}{4}=-\ln 2,\qquad(52a)$$

$$\langle S_i\cdot S_{i+2}\rangle-\frac{1}{4}=-4\ln 2+\frac{9}{4}\zeta(3).\qquad(52b)$$

The phase boundary between the CDW and the SDW phases is given by the equation[55]

$$E_{\mathrm{CDW}}=E_{\mathrm{SDW}}.\qquad(53)$$

The strong-coupling theory shows a good agreement with the Gaussian transition in the charge part, among the three transition lines that we have considered. We should also note that the present Gaussian critical point agrees with Cannon et al.'s result obtained by the direct evaluation of the CDW order parameter:[13] $V_c/t=1.65^{+0.10}_{-0.05}$ for $U/t=3$, and $V_c/t=2.92\pm0.04$ for $U/t=5.5$ (see Figs. 9 and 12).

From the above results, we conclude that the actual transition near the $U=2V$ line is not a direct CDW-SDW transition, but two independent Gaussian and spin-gap transitions, at least from the weak- to the intermediate-coupling region. In the strong-coupling region, these two boundaries approach and appear to be coupled at finite U and V. Unfortunately, in the present analysis, we cannot determine this tricritical point, but it is considered to be identical to the crossover point between the second- and the first-order transitions. This phenomenon is considered to be an effect of the charge-spin coupling term [the $g_{3\parallel}$ term in Eq. (6)] as was discussed by Voit in Ref. 4. In this way, our analysis suggests that the crossover along the $U=2V$ line is closely related to the validity of the charge-spin separation. Our result also demonstrates that there is a finite region of a charge- and spin-gapped state between the Gaussian and the spin-gap transition lines. It follows from the discussion in Sec. IV that the third phase is identified as a BCDW state.

In order to clarify the above interpretation for the CDW-SDW transition, we analyze the EHM including the correlated hopping term [Eq. (2)]. This term is known to enlarge the BCDW phase for $X/t<0$ even in the $U,V\to0$ limit, without disturbing the Y- and the I-shaped structure of the phase diagram for the charge and the spin parts (see Fig. 1). Because this term makes the magnitude of the backward and the Umklapp scattering couplings different [$g_{1\perp}=U-2V+4X/\pi,g_{3\perp}=-(U-2V-4X/\pi)$] conserving the SU(2)
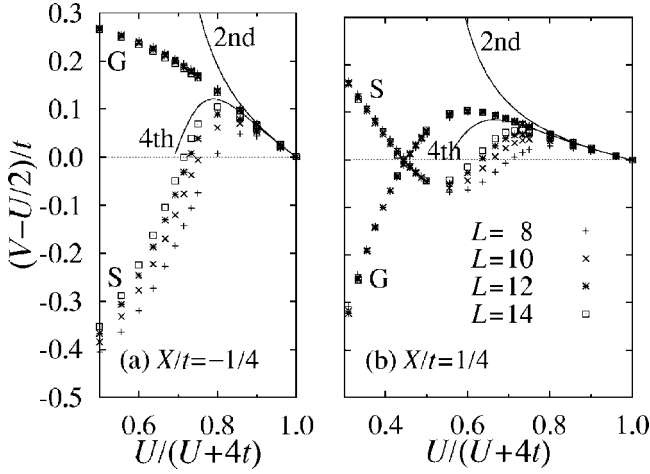
FIG. 13. The Gaussian (G) and the spin-gap (S) transitions in the strong-coupling region for (a) $X/t = -1/4$ and (b) $X/t = 1/4$. The strong-coupling theory [Eq. (53)] agrees with the Gaussian lines. Note that a BCDW phase appears not only in (a) but also in (b).

$\otimes$ SU(2) symmetry of the Hubbard model.[20] As was predicted by the g-ology, the BCDW phase appears from the weak- to the intermediate-coupling region.[56] On the other hand, in the strong-coupling region, the two transition lines are coupled, and the direct CDW-SDW transition takes place. The strong-coupling theory also agrees with the Gaussian line as is shown in Fig. 13(a). This is the same behavior as in the case of the pure EHM. Therefore, the tricritical point in the pure EHM is considered to have the same property of the one that separates the CDW, the SDW, and the BCDW phases in the case of $X/t < 0$.

For $X/t > 0$, the order of the Gaussian and the spin-gap transitions becomes vice versa, so that the BSDW phase appears. However, in Fig. 13(b), we find that the two transition lines cross in the intermediate-coupling region, and a finite BCDW phase appears. This BCDW region becomes narrower as the system size is increased. In the present analysis, we cannot conclude whether this BCDW phase remains or vanishes in the thermodynamic limit. We will consider this phenomenon again in Sec. VII.

D. Phase separation

Here, we determine the phase-separation boundary from the numerical data of the exact diagonalization.[57] Usually, the phase boundary is determined by the divergence of the compressibility.[58] However, for the $U/t \gg 1$ region of the EHM, the phase separation can take place in the SDW state where the compressibility cannot be defined. Consequently, the method of observing the divergence of the compressibility is no longer valid. In this paper, we determine the phase boundary by comparing the energy of the ground state and that of the phase-separated state. In the phase-separated state at half-filling, the system is separated into doubly occupied sites and a vacuum. In this case, the energy in the thermodynamic limit is exactly obtained as

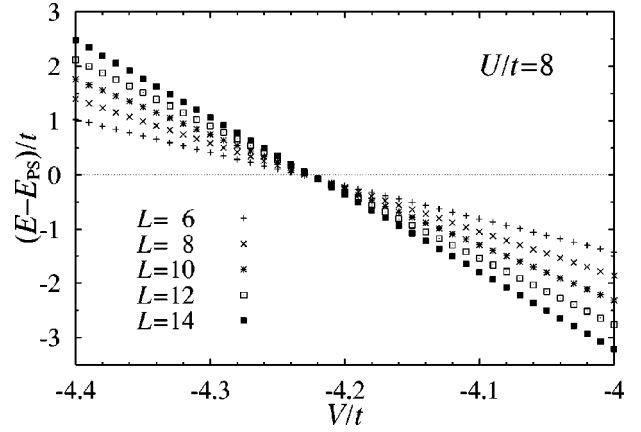$$E_{PS} = \frac{U + 4V}{2} L. \tag{54}$$

FIG. 14. Ground-state energy of the EHM for $L = 6 - 14$ systems at $U/t = 8$ measured from the fully phase separated state $E_{PS} = (U + 4V)L/2$ [Eq. (54)]. The zero point gives the critical point for the phase separation.

Therefore, we use the relation $E = E_{PS}$ as a criterion for the phase separation.[59] We show in Fig. 14 the ground-state energy of the EHM measured from the fully phase separated state. The zero point gives the critical point for the phase separation. The finite-size effect of the phase boundary is sufficiently small.

In order to check the validity of the numerical results, we compare our result with the asymptotic phase boundary in the strong-coupling limit. For $U/t \gg 1$ region, using Eqs. (51) and (54), the phase boundary is given by[10]

$$E_{PS} = E_{SDW}. \tag{55}$$

On the other hand, for $U/t \ll -1$ region, the system can be mapped onto the $S = 1/2$ XXZ spin chain with antiferromagnetic coupling $J_{xy} = 4t^2/|U|$ and $J_z = J_{xy} + 4V$, by using the η-pairing operators (20) and the second-order perturbation theory. Then, the phase boundary is given by $J_{xy} = -J_z$, which corresponds to the first-order transition between the XY and the ferromagnetic phases in the spin system.[8,9] If the effect of the correlated hopping term (2) is included, the phase boundary is given by

$$V = -\frac{2t^2}{|U|}(1 - \xi)^2. \tag{56}$$

The numerical result given by $E = E_{PS}$ well agrees with these asymptotic phase boundaries (see Fig. 15).

VI. QUARTER-FILLING

Finally, we analyze the phase diagram of the EHM at quarter-filling[23–25] by the level-crossing approach. In this case, the metal-insulator transition is considered as a BKT transition due to the higher-order Umklapp scattering ($q = 2$). Then, the phase boundary should be given by the level crossing between the marginal and four times of the $4k_F$-CDW spectra $x_{\rho 0} = 4x_{\rho 1}$ or $4x_{\rho 2} = x_{\rho 3}$, as was discussed in Sec. II B 2. In the present numerical analysis, we use the former level crossing, because $x_{\rho 3}$ needs larger Hilbert space than $x_{\rho 0}$ and $x_{\rho 2}$. Based on this assumption, we obtain the result shown in Fig. 16. Since the level-crossing point for the transition is higher ($x_\rho = 2$) than the case of the half-filling
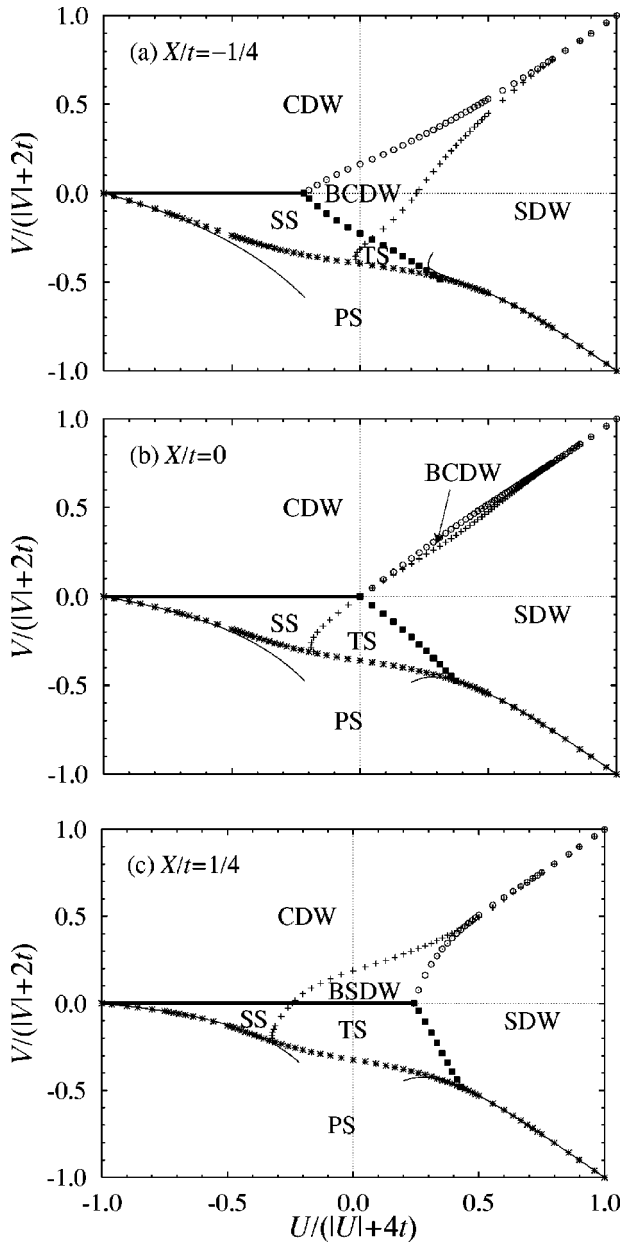
FIG. 15. Phase diagram of the 1D EHM determined by the data of the $L=12$ system at half-filling for (a) $X/t=-1/4$, (b) $X/t=0$, and (c) $X/t=1/4$ [CDW (SDW), charge (spin)-density wave; BCDW (BSDW), bond-charge (spin)-density wave; SS (TS), singlet (triplet) superconducting phase; PS, phase-separated state]. The asymptotic phase boundaries for the PS are given by Eqs. (55) and (56).

($x_\rho=1/2$), the finite-size effect from the irrelevant field (the deviation from the linearized dispersion relation) becomes larger. In this case, we need an extrapolation of the critical point to make the phase diagram. In the $U/t\to\infty$ limit, the transition point for the charge-gap phase is given by $V_c/t=2$, because it corresponds to the XY-Néel transition in the $S=1/2$ XXZ spin chain.[60,61] For the $U/t\gg1$ region, the extrapolated phase boundary flows into the point $(U,V)=(\infty,2t)$ as we expected. In order to check the consistency in the finite-U region, we calculate the following averaged scaling dimension:
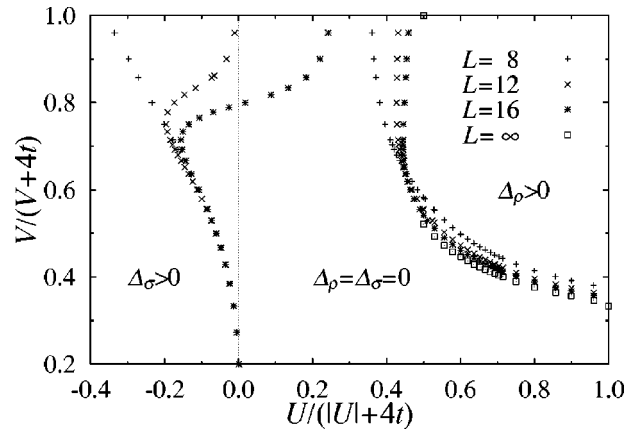

FIG. 16. Phase diagram of the 1D EHM at quarter-filling for the $V/t>0$ region. The phase boundary between the TL liquid and the $4k_F$-CDW phases is determined by the level crossing of $x_{\rho0}=4x_{\rho2}$ in $L=8,12,16$ systems. The critical points in the strong-coupling limits are $V_c/t=2$ and $U_c/t=4$, respectively.

$$\frac{x_{\rho1}+3x_{\rho2}}{4}=\frac{1}{2}. \tag{57}$$

Except for the large-V region, the extrapolated value becomes 1/2 with error less than 4%, as shown in Fig. 17. Thus, the universality class of the transition is considered to be a BKT-type.

On the other hand, for $V/t\gg1$ region, since the finite-size effect is too large, it is hard to perform the systematic extrapolation. However, the phase boundary appears to flow into the exact transition point $U_c=4t$ in the $V/t\to\infty$ limit as the system size is increased. Now let us review how the critical point of the charge-gap phase in the $V/t\to\infty$ limit is derived.[23] The charge gap is defined by

$$\Delta_\rho=E(N+1)+E(N-1)-2E(N). \tag{58}$$

At quarter-filling, $E(L/2)=0$. If one electron is add to this, then the energy is $E(L/2+1)=U$. Conversely, if one electron is removed, two free holes appear, then they have a kinetic energy $E(L/2-1)\sim-4t\cos(\pi/L)$. Therefore, the critical point for the charge-gap phase is given by $U_c=4t$ in the thermodynamic limit. We should note that the critical point in the $U/t\to\infty$ and $V/t\to\infty$ limits are given by a com-
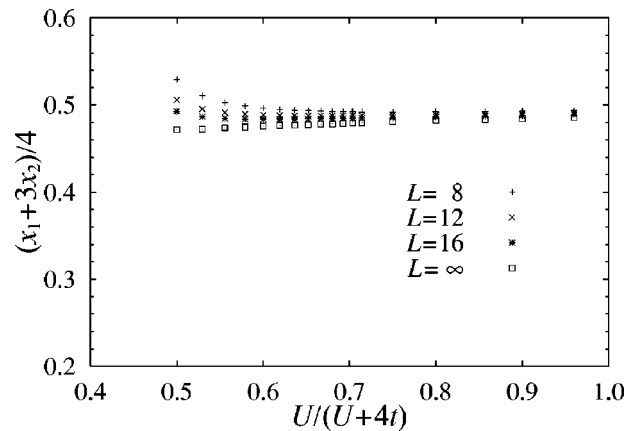

FIG. 17. Scaling dimensions given by Eq. (57) on the BKT line. The extrapolated value becomes 1/2 with error less than 4%.

pletely different argument. Therefore, we expect that a tricritical behavior may also be seen along the BKT transition line.

In a similar way as the half-filling, we consider the effect of a charge-spin coupling operator, which is derived from the $q=2$ Umklapp scattering between three parallel spins and one antiparallel spin [the $g_{3\parallel}$ term in Eq. (6)]. This operator may cause the synchronization of the BKT transition ($q=2$) in the charge part and the spin-gap transition. In order to examine this possibility, we determine the spin-gap phase boundary by the singlet-triplet level crossing in the large-V region. Then, the phase boundary of the spin gap appears to be coupled with that of the charge gap, and flows into the point $(U,V)=(4t,\infty)$, as the system size is increased. Therefore, this result suggests that the crossover in the metal-insulator transition also takes place by the mechanism similar to the case of half-filling. In the large-V region, there are phase-separated states,[26] but that has not been studied in the present analysis. We should also consider the effect of the phase separation in the future.

VII. SUMMARY AND DISCUSSION

Let us summarize the results obtained in this paper. We have determined the phase diagrams of the 1D EHM at half- and quarter-filling using the level-crossing approach, which is based on the TL liquid theory and the renormalization group. The metal-insulator transitions in half- (quarter-) filling are classified as BKT-type transitions due to the first- (second-) order Umklapp scattering. This fact reflects the ''fractional quantization'' discussed by the bosonization theory[27–30] and the generalized Lieb-Schultz-Mattis theorem.[29,30]

In the case of half-filling, for the charge sector, there are two BKT lines reflecting the SU(2) and hidden SU(2) symmetries, and one Gaussian line. These three critical lines meet at the multicritical point $(U/t,V/t)=(0,0)$, and they form a Y-shaped structure. Note that the same structure is also known in the phase diagram of the $S=1/2$ frustrated XXZ-spin chain.[62,32] For the spin sector, a spin-gap transition occurs due to the attractive backward scattering. Since the transition takes place at the origin of the RG flow diagram, the phase boundary has an I-shaped structure. Thus, the entire phase diagram is given by the combination of the ''Y'' and the ''I.''

The transition between the CDW and the SDW phases has been considered by assuming the following two scenarios: one is the independent Gaussian and spin-gap transitions under the charge-spin separation, the other is a direct CDW-SDW transition under the charge-spin coupling. By checking the relations between the scaling dimensions, and by comparing the numerical results with the strong-coupling theory, we have concluded that the first scenario is realized from the weak- to the intermediate-coupling ($U\sim4t$) region, and the second scenario is realized in the strong-coupling region. In the former case, a BCDW phase exists between the CDW and the SDW phases. Thus, the crossover of the CDW-SDW transitions from the second order to the first order turned out to be a phenomenon that reflects the validity of the charge-spin separation.

To clarify the mechanism of the crossover in more detail,

we have investigated the phase diagram of the EHM including the correlated hopping term (2). In this case, there appear BCDW and BSDW phases, depending on the order of the Gaussian and the spin-gap transitions. Note that the direct CDW-SDW transition also takes place in the strong-coupling region.

Therefore, we can understand the crossover of the CDW-SDW transition in the EHM as a kind of these generalized cases. The reason why the mechanism of the CDW-SDW transition has been left ambiguous for long times is that the analytical solutions both in weak- and strong-coupling limits give the same phase boundary $U=2V$, and the numerical analysis for the intermediate-coupling region does not have enough precision to distinguish the Gaussian and the spin-gap transition lines. Recently, the similar mechanism of transition was reported in studies of the Hubbard chain with periodic potential, which has the transition between Mott and band insulators.[63,64]

At quarter-filling, the phase boundary of the metal-insulator transition has also been determined by assuming that it is the BKT-type transition of the higher-order Umklapp scattering. The obtained phase boundary is consistent with the known exact results in the $U\to\infty$ and the $V\to\infty$ limits. In the present parameter space, there are neither a BKT transition with the hidden symmetry, nor a Gaussian transition. Although the finite-size effect in $V/t\gg1$ region is large, the phase boundaries of the charge- and the spin-gap phases appear to be coupled as the system size is increased. Therefore, there may be a crossover from the BKT to the first-order transitions in this region.

The rest of the section is devoted to discussions. We have clarified the mechanism of the CDW-SDW transition of the EHM at half-filling. However, we have not revealed the reason why the intermediate state in Figs. 12 and 15(b) is not a BSDW but a BCDW. We can interpret the appearance of the BCDW phase considering roles of the $g_{3\parallel}$ term in Eq. (6). When the charge gap opens in the $U>2V$ region ($g_{3\perp}^{*}=-\infty$), the phase field is locked as $\phi_{\rho}=2n\pi/\sqrt{8}$ with n being an integer, which minimize the classical potential energy associated with the $g_{3\perp}$ term. In this case, the charge part of the $g_{3\parallel}$ term is also locked, so that $g_{1\perp}=U-2V$ is reduced as

$$g_{1\perp}\to g_{1\perp}+g_{3\parallel}\langle\cos[\sqrt{8}\phi_{\rho}]\rangle, \qquad (59)$$

where $g_{3\parallel}=-2V$. Thus, if we estimate the spin-gap phase boundary in the weak-coupling region using Eq. (59), it shifts toward the $U>2V$ side of the $U=2V$ line. Similarly, we can estimate the shift of the Gaussian line. In the $U<2V$ region, the spin gap opens ($g_{1\perp}^{*}=-\infty$), then $g_{3\perp}=-U+2V$ shifts as

$$g_{3\perp}\to g_{3\perp}+g_{3\parallel}\langle\cos[\sqrt{8}\phi_{\sigma}]\rangle, \qquad (60)$$

where the phase field is locked as $\phi_{\sigma}=2n\pi/\sqrt{8}$. Therefore, the Gaussian line shifts toward the opposite side of the spin-gap phase boundary. Consequently, the BCDW phase appears between the CDW and the SDW phases. Thus, it turns out that the $g_{3\parallel}$ term enhances the BCDW phase when it is irrelevant, and it couples the Gaussian line and the spin-gap phase boundary when it is relevant. The deviations from the $U=2V$ line may be analyzed quantitatively in the weak-

coupling region by the renormalization group analysis including $g_{3\parallel}$. The above explanation may also be applicable to the phenomenon that a BCDW phase appears for $X/t>0$ in the strong-coupling region [see Fig. 13(b)].

We should consider the reason why the size dependence of the Gaussian transition line is smaller than that of the spin-gap phase boundary, in the strong-coupling region of Figs. 12 and 13. The reason is considered to be the difference between the behavior of the charge and the spin gaps. As was discussed in Sec. II, the spin gap opens exponentially slow (18), while the valley of the charge gap near the Gaussian transition becomes steeper as the strength of the interaction is increased (28). In the present analysis based on the TL liquid theory, we have assumed that both charge and spin parts are gapless, so that the Gaussian (spin-gap) transition line may be affected by the spin (charge) gap in the strong-coupling region. In the present case, magnitude and variation of the charge gap are considered to be much larger than those of the spin gap near the $U=2V$ line in the strong-coupling region, so that the Gaussian line has less size dependence than the spin-gap phase boundary.

In the present paper, we have not determined the tricritical point. This problem has been discussed by many authors.[6,11–13,4] Recently, the tricritical point is explored by the density-matrix-renormalization-group method,[15,65] but we may also determine the tricritical point by comparing the numerical result of the Gaussian transition line and the strong-coupling perturbative expansions in the higher order. It may also be worth studying the level crossing for the tricritical point by considering the logarithmic corrections to the excitation spectra, which stem from the $g_{3\parallel}$ term. In addition to the tricritical point between the CDW and the SDW phases, there is another tricritical point that separates the TS, the SDW, and the PS states. In Fig. 15, the phase boundaries between the SDW and the PS states obtained by the strong-coupling theory seem to be bent near the tricritical point. This tricritical point may also be identified by the further strong-coupling calculation.

Finally, we discuss the effect of site-off-diagonal interactions. In this paper, we have considered the correlated hopping term given by Eq. (2), however the generalized form of this term is given by[19]

$$\mathcal{H}_X = X \sum_{is} (c_{is}^\dagger c_{i+1,s} + \text{H.c.})(n_{i,-s} + n_{i+1,-s}), \quad (61a)$$

$$\mathcal{H}_{X'} = X' \sum_{is} (c_{is}^\dagger c_{i+1,s} + \text{H.c.}) n_{i,-s} n_{i+1,-s}. \quad (61b)$$

In the present paper, we have set $X=-X'/2$ to keep the particle-hole symmetry and the $\text{SU}(2) \otimes \text{SU}(2)$ symmetry of the Hubbard model. If this relation is not chosen, these symmetries are lost, so that the $V=0$ line is no longer the phase boundary of the metal-insulator transition at half-filling. Besides, an additional Umklapp term $\sin \sqrt{8}\phi_\rho$ appears in the effective Hamiltonian.[4,20] The analysis for this situation ($X \neq -X'/2$) is the subject of future research.

There are other types of site-off-diagonal interactions. For example, the bond-bond interaction term is given by[18]

$$\mathcal{H}_W = W \sum_{iss'} (c_{is}^\dagger c_{i+1,s} + \text{H.c.})(c_{is'}^\dagger c_{i+1,s'} + \text{H.c.}). \quad (62)$$

This term also makes the difference in the magnitude of the g parameters for the backward and the Umklapp scattering in the weak-coupling limit $[g_{1\perp} = U - 2V + 8W, g_{3\perp} = -(U - 2V - 8W)]$ (Ref. 4) conserving the symmetries of the Hubbard model. Therefore, we expect that this term play a role similar to the correlated hopping terms [Eq. (2)]. On the other hand, since this term can be rewritten as the exchange of the spins and of the pseudospins (20), it may affect the first-order transition to a ferromagnetic state[18] or the phase separation. Besides, in a parameter region of the EHM including this term, the BSDW state is shown to be the exact ground state.[66] The analysis of the effect of this term by the level-crossing approach will be reported elsewhere.[67]

APPENDIX A: WEAK-COUPLING LIMIT

In the weak-coupling limit, the parameters of the sine-Gordon model (6) can be identified in terms of the bare coupling constants of the original model, and consequently the phase boundaries are obtained analytically.[1–4,20] This approach is often called the g-ology.

The parameters of Eq. (6) are given by the g parameters defined in Refs. 2, 3, and 4 as follows:

$$v_\nu = \sqrt{u_\nu^2 - \left(\frac{g_\nu}{2\pi}\right)^2}, \quad K_\nu = \sqrt{\frac{2\pi u_\nu + g_\nu}{2\pi u_\nu - g_\nu}},$$

$$u_\nu \equiv v_F + \frac{g_{4\parallel} \pm g_{4\perp}}{2\pi}, \quad g_\nu \equiv g_{1\parallel} - g_{2\parallel} \mp g_{2\perp}, \quad (A1)$$

where the upper (lower) sign corresponds to $\nu = \rho$ ($\nu = \sigma$), and $v_F = 2t \sin(k_F)$ is the Fermi velocity. For the EHM including the X [Eq. (2)] and W [Eq. (62)] terms at half-filling, the g parameters can be identified as follows:

$$g_{1\perp} = g_\sigma = U - 2V + \delta g,$$

$$g_{3\perp} = -(U - 2V - \delta g),$$

$$g_\rho = -(U + 6V - \delta g), \quad (A2)$$

$$\delta g = 4X/\pi + 8W.$$

This calculation can be performed straightforwardly except for the X term. For the X term, which contains a three-body term, the operator-product-expansion technique is needed to identify the g parameters.[20]

The instabilities for the charge and the spin gaps are discussed based on the renormalization group (RG) analysis as explained in Sec. II. Since K_ν is approximated as $K_\nu \approx 1$

$+g_\nu/2\pi v_\nu$, the parameter in the RG flow diagram (Fig. 2) is given by $y_{0\nu}(l)=g_\nu/\pi v_\nu$. Then, the spin-gap opens when $g_{1\perp}=g_\sigma<0$, and the phase boundary is

$$U=2V-\delta g. \qquad (A3)$$

On the other hand, the charge gap opens when $g_{3\perp}>|g_\rho|$. The condition $g_{3\perp}=-g_\rho<0$ is the BKT-type transition due to the SU(2) symmetry in the charge sector. Then, the phase boundary is obtained as

$$V=0, \quad U<\delta g. \qquad (A4)$$

The condition $g_{3\perp}=g_\rho>0$ is the BKT-type transition due to the hidden SU(2) symmetry in the charge sector. Then, we obtain the phase boundary as

$$U=-2V+\delta g, \quad U>\delta g. \qquad (A5)$$

The Gaussian-type transition takes place at $g_{3\perp}=0$, for $g_\rho<0$. Thus, we obtain the Gaussian line for the charge sector as

$$U=2V+\delta g, \quad V<0. \qquad (A6)$$

Thus, we obtain the phase diagrams in the weak-coupling limit as is shown in Fig. 1, which have the Y- and the I-shaped structures in the charge and the spin degrees of freedom, respectively. In the present g-ology analysis, the parameters X and W appear only through δg, so that the X and W terms play similar roles in respect of the enhancement of the BCDW ($\delta g<0$) or the BSDW ($\delta g>0$) phases. The correspondence between the g-ology and the level-crossing approach is summarized in Table I.

In this paper, we have taken $U_{r,s}$ into account in the identification of $g_{1\perp}$ and $g_{3\perp}$ by following Ref. 40. The Clifford algebra for $U_{r,s}$ (5) can be expressed by tensor products of the Pauli matrices, which are chosen so the effective Hamiltonian (6) is to be diagonal in the space of $U_{r,s}$. For example, the following representation is possible:

$$U_{R\uparrow}=\tau^x\otimes\tau^x, \quad U_{R\downarrow}=\tau^z\otimes\tau^x,$$

$$U_{L\uparrow}=\tau^y\otimes\tau^x, \quad U_{L\downarrow}=1\otimes\tau^y. \qquad (A7)$$

These operators contribute to the $g_{1\perp}$ and the $g_{3\perp}$ terms as $\pm1\otimes\tau^z$, and one eigenvalue of the matrix is chosen. Consequently, the signs of $g_{1\perp}$ and $g_{3\perp}$ become opposite as in Eqs. (A2). When we consider the bosonization of a physical operator, it should be diagonalized simultaneously with the Hamiltonian. Therefore, if the physical operator cannot be diagonalized by Eq. (A7), we should choose other representations for $U_{r,s}$. In the derivation of the physical operators in Sec. IV, we need one more representation such as

$$U_{R\uparrow}=\tau^z\otimes\tau^x, \quad U_{R\downarrow}=\tau^x\otimes\tau^x,$$

$$U_{L\uparrow}=\tau^y\otimes\tau^x, \quad U_{L\downarrow}=1\otimes\tau^y. \qquad (A8)$$

In this case, the contribution to the $g_{1\perp}$ and the $g_{3\perp}$ terms is $\mp1\otimes\tau^z$. If the contribution of $U_{r,s}$ is neglected, the sign of the $g_{3\perp}$ term is reversed, and the roles of $\mathcal{O}_{\rho 1}$ and $\mathcal{O}_{\rho 2}$ are interchanged.

*Present address: Max-Planck-Institut für Physik komplexer Systeme, Nöthnitzer Str. 38 01187 Dresden, Germany.

[1] V. J. Emery, in *Highly Conducting One-Dimensional Solids*, edited by J. T. Devreese, R. Evrand, and V. van Doren (Plenum, New York, 1979), p. 327.

[2] J. Sólyom, Adv. Phys. **28**, 201 (1979).

[3] J. Voit, Rep. Prog. Phys. **57**, 977 (1995).

[4] J. Voit, Phys. Rev. B **45**, 4027 (1992).

[5] R. A. Bari, Phys. Rev. B **3**, 2622 (1971).

[6] J. E. Hirsch, Phys. Rev. Lett. **53**, 2327 (1984).

[7] P. G. J. van Dongen, Phys. Rev. B **49**, 7904 (1994).

[8] V. J. Emery, Phys. Rev. B **14**, 2989 (1976).

[9] M. Fowler, Phys. Rev. B **17**, 2989 (1978).

[10] H. Q. Lin and J. E. Hirsch, Phys. Rev. B **33**, 8155 (1985).

[11] B. Fourcade and G. Spronken, Phys. Rev. B **29**, 5089 (1984); **29**, 5096 (1984).

[12] J. W. Cannon and E. Fradkin, Phys. Rev. B **41**, 9435 (1990).

[13] J. W. Cannon, R. T. Scalettar, and E. Fradkin, Phys. Rev. B **44**, 5995 (1991).

[14] H. Q. Lin, E. R. Gagliano, D. K. Campbell, E. H. Fradkin, and J. E. Gubernatis, in *The Hubbard Model*, edited by D. Baeriswyl, D. K. Campbell, J. M. P. Carmelo, F. Guinea, and E. Louis (Plenum, New York, 1995), p. 315.

[15] G. P. Zhang, Phys. Rev. B **56**, 9189 (1997).

[16] M. Nakamura, J. Phys. Soc. Jpn. **68**, 3123 (1999).

[17] In the preceding works (Refs. 4 and 16), BCDW is called ''bond-order wave (BOW).''

[18] D. K. Campbell, J. Tinka Gammel, and E. Y. Loh, Jr., Phys. Rev. B **42**, 475 (1990).

[19] M. E. Simón and A. A. Aligia, Phys. Rev. B **48**, 7471 (1993).

[20] G. I. Japaridze and A. P. Kampf, Phys. Rev. B **59**, 12 822 (1999).

[21] A. A. Aligia, K. Hallberg, C. D. Batista, and G. Ortiz, Phys. Rev. B **61**, 7883 (2000); J. Low Temp. Phys. **117**, 1747 (1999).

[22] G. I. Japaridze, Phys. Lett. A **201**, 239 (1995).

[23] F. Mila and X. Zotos, Europhys. Lett. **24**, 133 (1993).

[24] K. Penc and F. Mila, Phys. Rev. B **49**, 9670 (1994).

[25] K. Sano and Y. Ōno, J. Phys. Soc. Jpn. **63**, 1250 (1994).

[26] R. T. Clay, A. W. Sandvik, and D. K. Campbell, Phys. Rev. B **59**, 4665 (1999).

[27] T. Giamarchi, Physica B **230-232**, 975 (1997).

[28] E. B. Kolomeisky and J. P. Straley, Rev. Mod. Phys. **68**, 175 (1996).

[29] M. Oshikawa, M. Yamanaka, and I. Affleck, Phys. Rev. Lett. **78**, 1984 (1997).

[30] M. Yamanaka, M. Oshikawa, and I. Affleck, Phys. Rev. Lett. **79**, 1110 (1997).

[31] K. Okamoto and K. Nomura, Phys. Lett. A **169**, 433 (1992).

[32] K. Nomura and K. Okamoto, J. Phys. A **27**, 5773 (1994).

[33] K. Nomura, J. Phys. A **28**, 5451 (1995).

[34] M. Nakamura, K. Nomura, and A. Kitazawa, Phys. Rev. Lett. **79**, 3214 (1997).

[35] M. Nakamura, J. Phys. Soc. Jpn. **67**, 717 (1998).

[36] M. Nakamura, A. Kitazawa, and K. Nomura, Phys. Rev. B **60**, 7850 (1999).

[37] R. J. Bursill, R. H. McKenzie, and C. J. Hamer, Phys. Rev. Lett. **80**, 5607 (1998).

[38] F. D. M. Haldane, J. Phys. C **14**, 2585 (1981).

[39] H. J. Schulz, Phys. Rev. Lett. **64**, 2831 (1990); Int. J. Mod. Phys. B **5**, 57 (1991).

[40] D. Sénéchal, e-print cond-mat/9908262.

[41] L. P. Kadanoff and A. C. Brown, Ann. Phys. (N.Y.) **121**, 318 (1979).

[42] J. M. Kosterlitz, J. Phys. C **7**, 1046 (1974).

[43] For example, see A. M. Tsvelik, *Quantum Field Theory in Condensed Matter Physics* (Cambridge University Press, Cambridge, 1995).

[44] I. Affleck, D. Gepner, H. J. Schulz, and T. Ziman, J. Phys. A **22**, 511 (1989).

[45] T. Giamarchi and H. J. Schulz, Phys. Rev. B **39**, 4620 (1989).

[46] A. A. Ovchinnikov, Zh. Éksp. Teor. Fiz. **57**, 2137 (1969) [Sov. Phys. JETP **30**, 1160 (1970)].

[47] H. Shiba, Prog. Theor. Phys. **48**, 2171 (1972).

[48] C. N. Yang and S. C. Zhang, Mod. Phys. Lett. B **4**, 759 (1990).

[49] V. L. Berezinskii, Zh. Éksp. Teor. Fiz. **61**, 1144 (1971) [Sov. Phys. JETP **34**, 610 (1972).

[50] J. M. Kosterlitz and D. J. Thouless, J. Phys. C **6**, 1181 (1973).

[51] J. L. Cardy, Nucl. Phys. B **270**, 186 (1986).

[52] P. Reinicke, J. Phys. A **20**, 5325 (1987).

[53] L. Hulthen, Ark. Mat., Astron. Fys. A **26**, 938 (1938).

[54] M. Takahashi, J. Phys. C **10**, 1289 (1977).

[55] We solved the equation numerically without using approximations. An approximation used in Ref. 7 is not appropriate for the quantitative analysis, as the author himself discussed. In the approximated case, the region where the CDW-SDW transition agrees with the Gaussian line is overestimated up to $U/t \sim 6$.

[56] In Ref. 22, the authors determined the phase diagram of the 1D Hubbard model ($V = 0$) including the correlated hopping term at half-filling [SU(2)⊗SU(2) symmetric case], by observing the quantum numbers corresponding to the current excitations (m_ν) using the Berry phase. Therefore, if the SU(2) symmetry in the charge sector is broken ($V \neq 0$), their method may correspond to the level crossing of the Gaussian-type transition, but may not correspond to the one of the BKT-type transition.

[57] In Ref. 10, the authors calculated the phase-separation boundary in the 1D EHM by observing the divergence of the spin susceptibility at wave number $q = \pi$ using the Monte Carlo simulation.

[58] M. Ogata, M. U. Luchini, S. Sorella, and F. F. Assaad, Phys. Rev. Lett. **66**, 2388 (1991).

[59] This method is equivalent to the way of determining the critical points for the dimer-ferromagnet and the XY-ferromagnet transitions in the $S = 1/2$ frustrated XXZ spin chain; S. Hirata and K. Nomura, Phys. Rev. B **61**, 9453 (2000).

[60] A. A. Ovchinnikov, Zh. Éksp. Teor. Fiz. **64**, 342 (1972) [Sov. Phys. JETP **37**, 176 (1973)].

[61] A. Luther and I. Peschel, Phys. Rev. B **12**, 3908 (1975).

[62] F. D. M. Haldane, Phys. Rev. B **25**, 4925 (1982); **26**, 5257 (1982).

[63] M. Fabrizio, A. O. Gogolin, and A. A. Nersesyan, Phys. Rev. Lett. **83**, 2014 (1999).

[64] Y. Takada and M. Kido, e-print cond-mat/0001239 (unpublished).

[65] In Ref. 15, the phase boundary between the CDW and the SDW phases is determined by observing the CDW and the SDW structure factors using the density-matrix-renormalization-group method. This result agrees with our level-crossing point of the CDW and the SDW excitations.

[66] K. Itoh, M. Nakamura, and N.Muramoto (unpublished).

[67] M. Nakamura, K. Itoh, and N. Muramoto, cond-mat/0003419.